THE ASTROPHYSICAL JOURNAL, 539:1002–1022, 2000 August 20

A METHOD TO DETERMINE THE HEATING MECHANISMS OF THE SOLAR CORONA

E. R. PRIEST,[1] C. R. FOLEY,[2] J. HEYVAERTS,[3] T. D. ARBER,[1] D. MACKAY,[1]
J. L. CULHANE,[2] AND L. W. ACTON[4]
Received 1998 June 4; accepted 2000 February 24

ABSTRACT

One of the paradigms about coronal heating has been the belief that the mean or summit temperature of a coronal loop is completely insensitive to the nature of the heating mechanisms. However, we point out that the temperature profile along a coronal loop is highly sensitive to the form of the heating. For example, when a steady state heating is balanced by thermal conduction, a uniform heating function makes the heat flux a linear function of distance along the loop, while $T^{7/2}$ increases quadratically from the coronal footpoints; when the heating is concentrated near the coronal base, the heat flux is small and the $T^{7/2}$ profile is flat above the base; when the heat is focused near the summit of a loop, the heat flux is constant and $T^{7/2}$ is a linear function of distance below the summit. It is therefore important to determine how the heat deposition from particular heating mechanisms varies spatially within coronal structures such as loops or arcades and to compare it to high-quality measurements of the temperature profiles.

We propose a new two-part approach to try and solve the coronal heating problem, namely, first of all to use observed temperature profiles to deduce the form of the heating, and second to use that heating form to deduce the likely heating mechanism. In particular, we apply this philosophy to a preliminary analysis of *Yohkoh* observations of the large-scale solar corona. This gives strong evidence against heating concentrated near the loop base for such loops and suggests that heating uniformly distributed along the loop is slightly more likely than heating concentrated at the summit. The implication is that large-scale loops are heated in situ throughout their length, rather than being a steady response to low-lying heating near their feet or at their summits. Unless waves can be shown to produce a heating close enough to uniform, the evidence is therefore at present for these large loops more in favor of turbulent reconnection at many small randomly distributed current sheets, which is likely to be able to do so. In addition, we suggest that the decline in coronal intensity by a factor of 100 from solar maximum to solar minimum is a natural consequence of the observed ratio of magnetic field strength in active regions and the quiet Sun; the altitude of the maximum temperature in coronal holes may represent the dissipation height of Alfvén waves by turbulent phase mixing; and the difference in maximum temperature in closed and open regimes may be understood in terms of the roles of the conductive flux there.

Subject heading: Sun: corona

1. INTRODUCTION

The question about what mechanisms are heating the solar corona is a fundamental one in astrophysics that has defied physicists for half a century (e.g., Ulmschneider, Priest, & Rosner 1991). We are now at a key point in our attempts to answer it and hence in our understanding of the solar corona. The Japanese/US/UK *Yohkoh* satellite has been in operation for over 7 yr and has produced unprecedented detail on the complex interaction of coronal structures. We need therefore to absorb thoroughly the implications of these spectacular observations for our overall understanding of how the corona is heated so as to appreciate which parts of the coronal heating puzzle have been solved and which parts remain. At the same time, the ESA-NASA *SOHO* satellite is working well, so we need to decide on the best ways of using *SOHO*, the *Transition Region and Coronal Explorer* (*TRACE*), and future missions such as *Solar B* to tackle the coronal heating problem.

The recognition that the global or summit temperature of a coronal loop is completely insensitive to the nature of the heating (Chiuderi, Einaudi, & Toricelli-Ciamponi 1981) led to fears that we would not be able to determine the nature of the heating mechanisms. In addition, we have developed many models for the ways in which MHD waves behave or current sheets form without being able to relate them to observations of the corona.

The fact that, as we shall demonstrate here, the shape of the temperature profile along a coronal loop and within a coronal arcade is highly sensitive to the nature of the heating opens a new door to deduce the heating mechanisms. In turn, this is a stimulus to deduce the form of the heating produced by different mechanisms and to measure temperature profiles in coronal structures with as small an error as possible.

In this paper, we review briefly the different theories (§ 1.2) and observations (§ 1.3) of coronal loops. We then propose a new technique for trying to identify coronal heating mechanisms building on the pioneering work of Kano & Tsuneta (1996). We develop simple models for the temperature structure above a million degrees Kelvin of coronal loops (§ 2) and coronal arcades (§ 3). Next, we compare the models with observed data on a large-scale loop and arcade from *Yohkoh* and are able to determine the likely form of the mechanism that is heating the large-scale

[1] Department of Mathematical and Computational Sciences, St. Andrews University, St. Andrews KY16 9SS, Scotland.
[2] Observatoire, 11 Rue de l'Université, F-67000 Strasbourg, France.
[3] Mullard Space Science Laboratory, University College London, Holmbury St. Mary, Dorking, Surrey RH5 6NT, UK.
[4] Department of Physics, Montana State University, Bozeman, MT 59717.

corona (§ 4). We also apply a similar technique to coronal hole data (§ 5) and consider basic questions about the global behavior of the solar corona (§ 6). Finally, we suggest a strategy for tackling some of the remaining pieces of the coronal heating jigsaw (§ 7).

1.1. *The Nature of the Solar Corona*

The corona consists of three distinct types of structure when viewed in soft X-rays at moderate resolution (e.g., from *Skylab*), namely,

1. *X-ray–bright points*, which are tiny intense regions lasting for typically 8 hr and lying above oppositely directed magnetic fragments in the photosphere;
2. *coronal loops*, where the magnetic field is closed and is able to contain regions of high density; and
3. *coronal holes*, where the magnetic field is open, the plasma density is low, and from which the fast solar wind escapes.

The traditional unproved paradigm of coronal heating has been that these three types of structure are likely to be heated by three different mechanisms. The majority feeling has been that it is reasonable to expect that X-ray–bright points are likely to be heated by new magnetic flux emerging from below the photosphere and reconnecting with the overlying field; coronal loops are likely to be heated by the dissipation of electric currents driven by footpoint motions, for example, by nanoflares in current concentrations produced by magnetic braiding, as in the nanoflare model that Parker (1994) has developed in a convincing manner; and coronal holes are likely to be heated by Alfvén waves, because no other mechanism has seemed possible.

However, several parts of this paradigm have been recently challenged. First, most X-ray–bright points are now known to lie above flux that is cancelling rather than emerging (Harvey 1984). This has led to a convincing answer to the question what heats them, since the Cancelling Flux Model has explained their observational properties in a natural way in terms of magnetic reconnection driven by footpoint motions (Priest, Parnell, & Martin 1994). Nevertheless, the mechanisms for heating the coronal loops and coronal holes have not yet been identified, despite several attempts to propose observational tests (Jordan 1992; Mason 1995; Waljeski, Dere, & Moses 1992; Zirker 1993; Cargill 1994a). Second, *Yohkoh* observations (Tsuneta 1996) have demonstrated that the heating of coronal loops possesses two distinct components, splitting the second element of the above classification into two parts, namely,

2a. steady heating of coronal loops, which provides a basal or background level, and
2b. impulsive heating of coronal loops, which raises the temperature sporadically above the background.

Furthermore, it may well be the case that different kinds of loop are heated by different mechanisms, although it would be simpler and more elegant if only one mechanism were dominant throughout the corona: if this were the case, then the X-ray–bright point results would favor magnetic reconnection (e.g., Priest & Forbes 2000).

1.2. *Theories of Coronal Heating*

Theories for coronal heating have been reviewed by several authors and fall into three different types, namely, bright-point heating, wave heating, and (possibly turbulent) current sheet heating (Hollweg 1983; Heyvaerts 1990; Cargill 1994b; Vlahos 1994; Priest 1993, 1996). First of all, a viable canceling flux model of how most bright points are heated has been given by Priest et al. (1994), in which the motion of photospheric fragments drives reconnection in the overlying corona. It has been compared in detail with observations of particular bright points from NIXT (Parnell, Golub, & Priest 1994) and explains their internal structure.

Second, the properties of Alfvén waves have been studied in detail by Hollweg (1983), Roberts (1984), Goossens (1991), Goedbloed (1983), Porter, Klimchuk, & Sturrock (1994), and Klimchuk & Porter (1995). One way of dissipating shear Alfvén waves is by phase mixing (e.g., Heyvaerts & Priest 1983; Sakurai 1985; Cally 1991; Hood, Ireland, & Priest 1997), while other MHD modes may suffer resonant absorption (Tataronis & Grossman 1973; Goedbloed 1983; Poedts, Kerner, & Goossens 1989; Steinolfson & Davila 1993; Ofman, Davila, & Steinolfson 1995).

A third class of theories is current-sheet heating. In coronal loops and arcades, slow footpoint motions make the coronal magnetic field try to evolve through a series of equilibrium configurations. Often, however, the equilibria are not smooth but contain current concentrations (sometimes singular) where dissipation can occur either directly or indirectly at reconnection sites by conversion of magnetic energy into kinetic energy, which eventually dissipates in turbulent plasma motions (e.g., Hendrix & Van Hoven 1996; Einaudi et al. 1996). There are several ways of forming such sheets, namely, driven reconnection and flux interaction, braiding, X-point collapse and shearing (Parker 1979, 1990; Low & Wolfson 1988; Vekstein & Priest 1992). A recent numerical experiment on braiding by Galsgaard & Nordlund (1996) shows that the field lines are braided by one turn before they reconnect and that the resulting time-averaged heating is rather uniform in many small current sheets distributed through the medium (Galsgaard et al. 1999).

Many coronal heating mechanisms, such as braiding and current sheet formation or resistive instabilities or waves, all lead to a state of MHD turbulence. Heyvaerts & Priest (1984) made a start at analyzing it by adapting Taylor's relaxation theory to the coronal environment, in which the field lines thread the boundary rather than being parallel to it. Later, Heyvaerts, & Priest (1993) developed a new approach in which the level of coronal turbulence is self-consistently calculated.

1.3. *Observations of Coronal Loops*

Observations from the Soft X-Ray Telescope (SXT) on board the Japanese *Yohkoh* satellite have revealed that the corona is a complex magnetohydrodynamic system that is highly time dependent and three dimensional (Ogawara et al. 1991; Uchida 1993; Tsuneta 1996; Culhane 1997), with myriads of magnetic loops continually evolving and interacting. These observations have also given important clues as to how the corona is heated. In particular, a distinction has been revealed between local, time-dependent impulsive components to the heating and global, steadier components on a much larger scale (Tsuneta 1996; Acton 1996).

For example, in active regions there are tiny transient brightenings (Shimizu et al. 1992), which are likely to be driven by reconnection between multiple loops (like X-ray–

bright points), but they fall short by a factor 5–10 of being able to heat active-region loops. Furthermore, the hottest loops in active regions (6–7 MK) appear to be multiple structures that are interacting by reconnection or tiny cusplike features (Tsuneta 1996; Yoshida & Tsuneta 1996), which may represent loops that are closing down by reconnection. Also, Shibata et al. (1995) have observed many examples of X-ray jets accelerated from a variety of structures. On a large scale too there is a transient component in the form of enormous cusp-shaped structures that form after global eruptions associated with eruptive prominences and coronal mass ejections (Tsuneta et al. 1992; Tsuneta & Lemen 1993). Indeed, MacAllister (1999, private communication) finds that most of the strongest coronal arcades above large-scale polarity inversion lines at high latitudes have formed in this manner.

Kano & Tsuneta (1996), Yoshida et al. (1995), Ichimoto et al. (1995) find that the X-ray temperatures within active regions range from 3 to 10 MK. The loop structures with shorter lifetimes (less than a few hours) generally have high temperatures and represent plasma transiently heated by reconnection (Tsuneta 1996). By contrast, loops with longer lifetimes are cooler, with temperatures of 2–4 MK, and represent plasma that is heated more steadily and uniformly with a lifetime of 1 day or longer (Tsuneta 1996). Kano & Tsuneta (1996) have obtained the temperature distribution along steady loops and find two types, namely, profiles of trapezoidal or triangular type. In the latter case the conductive flux is constant either side of a localized region of heat input. Also, Neupert et al. (1998) have used *SOHO* EIT observations to study the structure of loops above an active region. In quiet regions Krucker & Benz (1998) have shown that EIT brightenings have a power law that is steep enough to give nanoflares enough energy to heat the corona (if they do continue down at the same rate to small enough events). Parnell & Jupp (2000) have repeated the analysis using *TRACE* data for very much smaller events and find that the spectrum does continue down at the same rate and that it would need to continue down to energies of 4×10^{24} ergs to provide the heating.

On larger scales weaker emission has been observed with *Yohkoh* from large closed regions that extend up to 0.8 $R_\odot$ above the limb and underlie coronal streamers. For example, Sturrock, Wheatland, & Acton (1996) studied a large magnetically closed region of the diffuse corona and from filter ratios they deduced that the temperature increases with radius from 1.6 MK at the limb to 2.3 MK at 1.5 $R_\odot$. They modeled this temperature variation approximately by assuming that the heat flux is constant and the field lines radial. In § 5 we present new observations with lower errors and model them in a more realistic way.

Yohkoh observations of coronal holes on the disc have been reported by Hara et al. (1994), who evaluated the temperature and emission measure from observations of equatorial holes on the disc and included a correction for X-ray scattering by the telescope mirrors from sources of emission visible on the rest of the solar surface. They found temperatures for the individual coronal holes in the range 1.8–2.4 MK, which were similar to the values found for the nearby quiet corona, while the electron density values were about three times lower. More recently, Foley, Culhane, & Acton (1997) have investigated the limb temperatures of coronal holes and find them to be 1.1 MK at the limb and 1.35 MK at 1.15 $R_\odot$, which are lower than those reported by Hara. By comparison the temperature of the "quiet" Sun outside active regions and coronal holes is about 2 MK (Tsuneta 1996).

2. CORONAL LOOP MODELS

Consider the coronal part of a loop of cross-sectional area A and temperature T in energy balance between thermal conduction and heating such that

$$\frac{1}{A(s)}\frac{d}{ds}\left[A(s)\kappa_0 T^{5/2}\frac{dT}{ds}\right] = -H\,, \tag{2.1}$$

where s is the distance along the loop from one coronal footpoint, $\kappa_0 T^{5/2}$ is the coefficient of thermal conduction (with $\kappa_0 = 9.24 \times 10^{-12}$ J m^{-1} s^{-1}), and H is the heating rate per unit volume. Thus, in order of magnitude, the conduction has magnitude $\kappa_0 T^{7/2}/L^2$, where $2L$ is the loop length, and the optically thin radiation may be written as $n_e^2 \chi T^\alpha$ in terms of the density (n_e) and temperature-dependent parameters χ and α. Radiation is therefore negligible above a critical temperature ($T_{\rm crit}$), which is typically 10^6 K for a loop having a half-length of 100 Mm and a density of $10^{8.5}$ cm^{-3}, say (Fig. 1*a*).

Equation (2.1) may be integrated in general to give the heat flux (which is negative) as

$$F(s) \equiv -\kappa_0 T^{5/2}\frac{dT}{ds} = -\frac{1}{A(s)}\int_s^L H(s')A(s')ds'\,, \tag{2.2}$$

assuming that the temperature gradient dT/ds vanishes at the loop summit ($s = L$). This in turn may be integrated to give the temperature $[T(s)]$ as a function of distance along the loop as

$$\begin{aligned} T &= T_0\left[1 - \frac{7}{2\kappa_0 T_0^{7/2}}\int_0^s F(s')ds'\right]^{2/7} \\ &= T_0\left[1 + \int_0^s \frac{7}{2\kappa_0 A(s')T_0^{7/2}}\,ds' \right. \\ &\quad \left. \times \int_{s'}^L H(s'')A(s'')ds''\right]^{2/7}\,, \end{aligned} \tag{2.3}$$

where T_0 the temperature at the coronal base of one footpoint ($s = 0$).

Now let us examine the effect of different forms of heating on the heat flux and temperature profile, in each case taking the loop area constant and assuming symmetry in loop properties about the summit for simplicity. Many loops are observed to have remarkably uniform cross sections (Klimchuk et al. 1992), but the theory can easily be generalized to include area variations. First of all, suppose the heating is uniform along the loop $[H(s) = H_0]$. Then the heat flux becomes a distinctive linear function of s,

$$F(s) = -H_0(L - s)\,, \tag{2.4}$$

in which the base value $[F_0 = -F(0) = H_0 L]$ is a direct measure of the strength (H_0) of the heating. The temperature is given in turn by

$$T(s) = T_0\left(1 + \overline{H}\,\frac{Ls - s^2/2}{L^2}\right)^{2/7}\,, \tag{2.5}$$

where the parameter

$$\overline{H} = \frac{7H_0 L^2}{2\kappa_0 T_0^{7/2}} \tag{2.6}$$

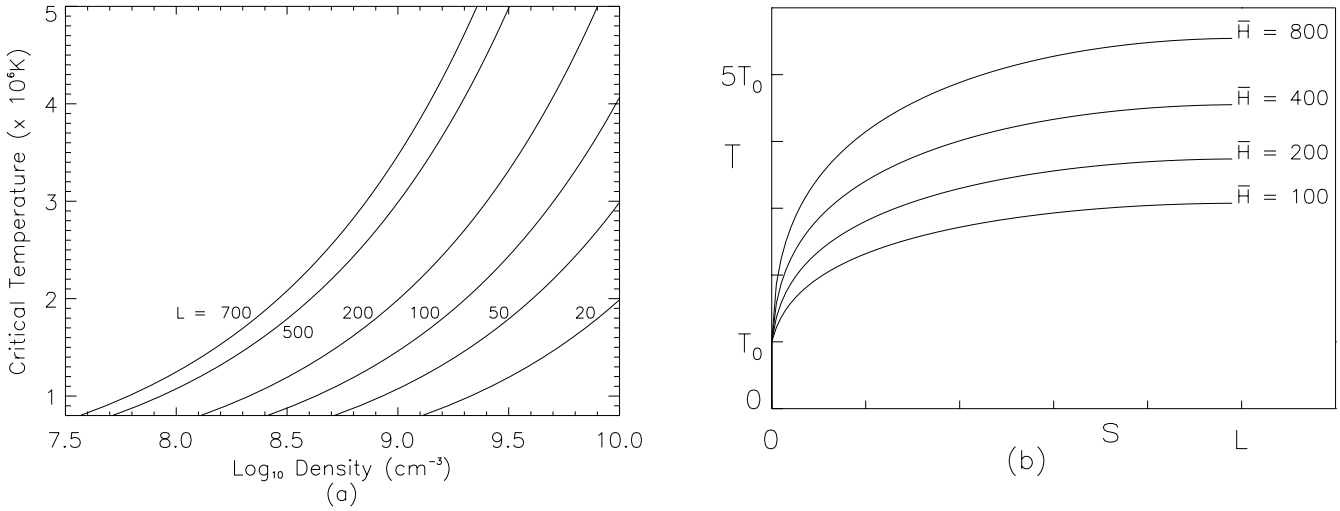

FIG. 1.—(*a*) Dependence of the critical temperature (T_{crit}) above which conduction dominates radiation on loop density for different loop half-lengths L (in Mm) indicated on each curve. (*b*) Temperature (T) as a function of distance (s) along a loop from coronal base ($s = 0$) to summit ($s = L$) and its dependence on the heating parameter $\overline{H} = 7H_0 L^2/(4\kappa_0 T_0^{7/2})$ when the heating (H_0) is uniform.

is a measure of the ratio of heating to conduction and its effect on the temperature profile is shown in Figure 1*b*. The maximum (i.e., summit) temperature is

$$T_m = T_0(1 + \tfrac{1}{2}\overline{H})^{2/7} . \tag{2.7}$$

It can be seen how an increase in heating (H_0) causes the heat flux (Fig. 2*a*, *dotted curve*) and temperature (Fig. 1*b*) to increase and how the characteristic of uniform heating is that $T^{7/2}$ increases parabolically with s.

Second, suppose the heating is uniform over a distance L_H from the base. Then the heat flux,

$$F(s) = \begin{cases} -H_0(L_H - s) , & s < L_H , \\ 0 , & s > L_H , \end{cases} \tag{2.8}$$

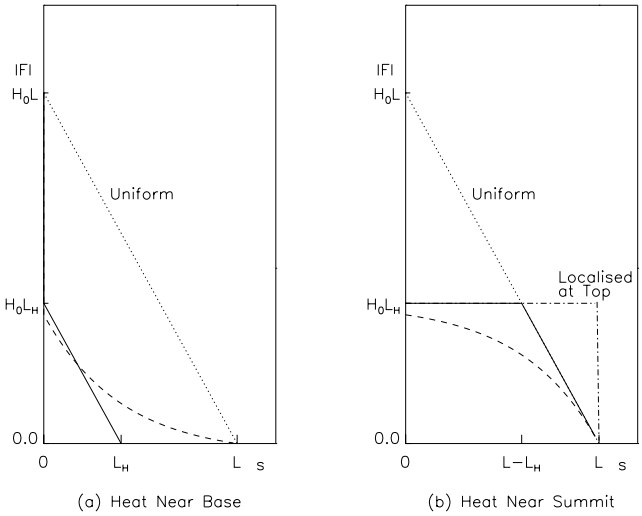

FIG. 2.—Absolute value of the heat flux ($-F$) as a function of distance (s) along a loop is shown as a solid curve when (*a*) the heating (H_0) is uniform for a distance L_H from the base; (*b*) the heating is uniform over a distance L_H from the summit (with the limit $L_H \to 0$ while $H_0 L_H = f_0$ is held constant; *dot-dashed line*). In both cases the examples of uniform heating over the whole loop and of heating decaying away exponentially from the base or summit are shown by dotted and dashed lines, respectively.

is a linear function up to the point L_H and zero beyond (Fig. 2*a*, *solid curve*), while the base value is now $F_0 = H_0 L_H$.

The decrease in the total heat deposited in the loop for the same value of H_0 therefore reduces the heat flux everywhere in the heated part of the loop by a factor L_H/L. The resulting temperature profile (Fig. 3*a*, *solid curve*) is

$$T(s) = \begin{cases} T_0\left(1 + \overline{H}\,\dfrac{L_H s - s^2/2}{L^2}\right)^{2/7} , & s < L_H < L , \\ T_m , & L_H < s < L , \end{cases} \tag{2.9}$$

where

$$T_m = T_0(1 + \tfrac{1}{2}\,\overline{H} L_H^2/L^2)^{2/7} \tag{2.10}$$

is the maximum (i.e., summit) temperature. Thus, as well as creating a flat temperature profile near the summit, this form of heating lowers the temperature gradient and the temperature in the lower portion of the loop.

For the third type of heating suppose the heating is uniform over a distance L_H either side of the summit. This produces a heat flux of

$$F = \begin{cases} -H_0 L_H , & 0 < s \le L - L_H , \\ -H_0(L - s) , & L - L_H < s \le L , \end{cases} \tag{2.11}$$

which therefore has the same profile as the uniform heating case near the summit but is truncated near the base to the constant value ($H_0 L_H$) that represents the total heat deposited in the half-loop (Fig. 2*b*, *solid curve*). When $L > L_H$, the temperature profile now becomes

$$T(s) = \begin{cases} T_0\left(1 + \overline{H}\,\dfrac{L_H s}{L^2}\right)^{2/7} , & 0 \le s \le L - L_H , \\ T_0\left\{1 + \overline{H}\left[\dfrac{s}{L} - \dfrac{s^2}{2L^2} - \dfrac{(L - L_H)^2}{2L^2}\right]\right\}^{2/7} , & \\ & L - L_H < s \le L . \end{cases} \tag{2.12}$$

When $L < L_H$, the loop temperature reverts to that of the uniform case (eq. [2.5]).

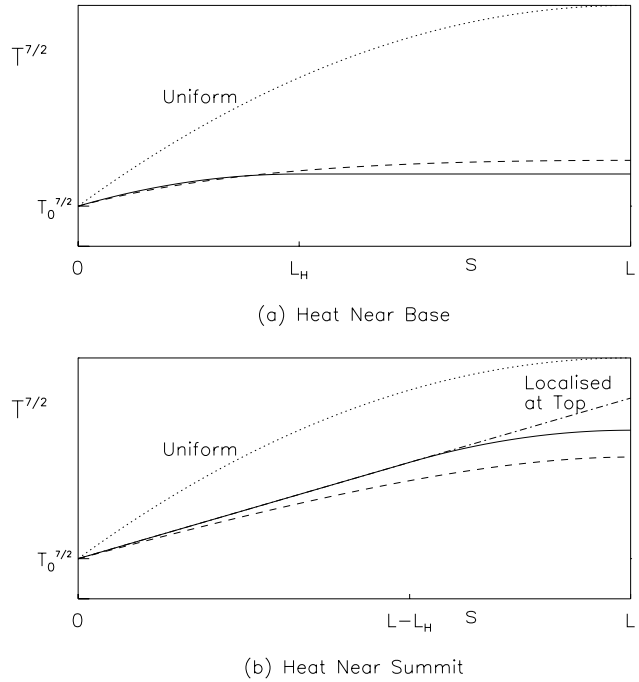

FIG. 3.—Temperature profile $T(s)$ along a loop when the heating is (*a*) uniform (*dotted line*), uniform over a length L_H from the footpoint (*solid line*) or is of the form $H = H_0 \exp(-s/L_H)$ decaying over a distance L_H from the footpoint (*dashed line*); (*b*) uniform over a length L_H from the summit (*solid line*) or concentrated at the summit (*dot-dashed line*) or of the form $H_0 \exp[(s-L)/L_H]$ decaying over a distance L_H from the summit (*dashed line*).

As shown in Figure 3*b* (*solid curve*), $T^{7/2}$ therefore has a linear profile in the region of no heating and a quadratic profile where the heat is uniformly deposited. The maximum temperature is

$$T_m = T_0\left[1 + \overline{H}\left(\frac{L_H}{L} - \frac{L_H^2}{2L^2}\right)\right]^{2/7}, \tag{2.13}$$

so, when $L_H \ll L$, this is roughly the same form as equation (2.7) for uniform heating but with the heat parameter $\overline{H}$ reduced by a factor $2L_H/L$ because of the reduction in the amount of heat deposited in the loop and of the heat flux near the base. Furthermore, the summit temperature (eq. [2.13]) is always smaller than the corresponding value (eq. [2.7]) for uniform heating when $L_H < L$.

Fourth, consider the limit when L_H approaches zero in case three but with $H_0 L_H = f_0$, say, held constant so that we have a finite amount of heat deposited right at the top of the loop. Then the heat flux is a constant

$$F = -f_0, \quad 0 \le s < L, \tag{2.14}$$

and the temperature is simply

$$T(s) = T_0\left(1 + \frac{7 f_0 s}{2\kappa_0 T_0^{7/2}}\right)^{2/7}. \tag{2.15}$$

Thus the function $T^{7/2}$ increases linearly from base to summit (Fig. 3*b*, *dot-dashed curve*), where the temperature reaches

$$T_m = T_0\left(1 + \frac{7 f_0 L}{2\kappa_0 T_0^{7/2}}\right)^{2/7}, \tag{2.16}$$

so we have the same result as in equation (2.13) but without the quadratic term. This temperature maximum is smaller than the uniform heating case (eq. [2.7]) when $L_H < \frac{1}{2}L$.

The effect of two other forms of heating is described in Appendix A, namely, when the heating is decaying exponentially away from the feet or summit.

3. CORONAL ARCADE MODELS

Now consider an arcade of coronal loops, one above another, in each of which the temperature $T(s)$ is given by equation (2.3). How does the temperature variation with altitude at the summits of the loops depend on the form of the heating within each loop and the way the net heating varies from one loop to another? The summit temperature (T_s) is given simply by $T(L)$, so, when the heating is uniform along each loop but is allowed to vary from one loop to another, equation (2.5) implies that

$$T_s = T_0(1 + \frac{1}{2}\overline{H})^{2/7}. \tag{3.1}$$

If the heating is the same per unit volume for all loops, so that $\overline{H} \sim L^2$, this shows how T_s increases with L. For a set of semicircular loops, for example, $L = \pi h/2$, so it may be converted to

$$T_s = T_0\left(1 + c_H \frac{h^2}{R_\odot^2}\right)^{2/7} \tag{3.2}$$

for the variation of summit temperature with height (h), where $c_H = 7H_0 R_\odot^2 \pi^2/(16\kappa_0 T_0^{7/2})$.

If instead the base heating flux ($F_0 = H_0 L$) is the same for each loop and the heating is uniform within each loop, then

$$T_s = T_0\left(1 + c_F \frac{h}{R_\odot}\right)^{2/7}, \tag{3.3}$$

where $c_F = 7F_0 R_\odot \pi/(8\kappa_0 T_0^{7/2})$. Thus a clear distinction between uniform-heat and uniform-flux arcades is that in the former case $T_s^{7/2}$ increases quadratically with height whereas in the latter it increases linearly (Figs. 4*a* and 4*b*, *dotted curves*).

3.1. *Semicircular Arcade*

Next let us consider the effect on a similar arcade of the different forms of heating considered in the previous section. If the heating is uniform over a distance L_H along the loop from the base, so that the temperature in each loop of the arcade is of the form of equation (2.10), then the summit temperature in the arcade becomes (Fig. 4*a*, *solid curve*)

$$T_s = \begin{cases} T_0(1 + c_H h^2/R_\odot^2)^{2/7}, & h < h_H, \\ T_0(1 + c_H h_H^2/R_\odot^2)^{2/7}, & h > h_H, \end{cases} \tag{3.4}$$

where $h_H = 2L_H/\pi$ is the height in the arcade below which the arcades are uniformly heated (Fig. 5*b*). For uniform-flux arcades the corresponding profile (Fig. 4*b*, *solid curve*) is

$$T_s = T_0 \begin{cases} (1 + hc_F/R_\odot)^{2/7}, & h < h_H, \\ (1 + h_H c_F/R_\odot)^{2/7}, & h > h_H. \end{cases} \tag{3.5}$$

Thus the characteristic feature of this type of heating is that it flattens off the temperature profile above the height h_H.

Third, consider a heating that is deposited uniformly over a distance L_H either side of the summit of each loop in the

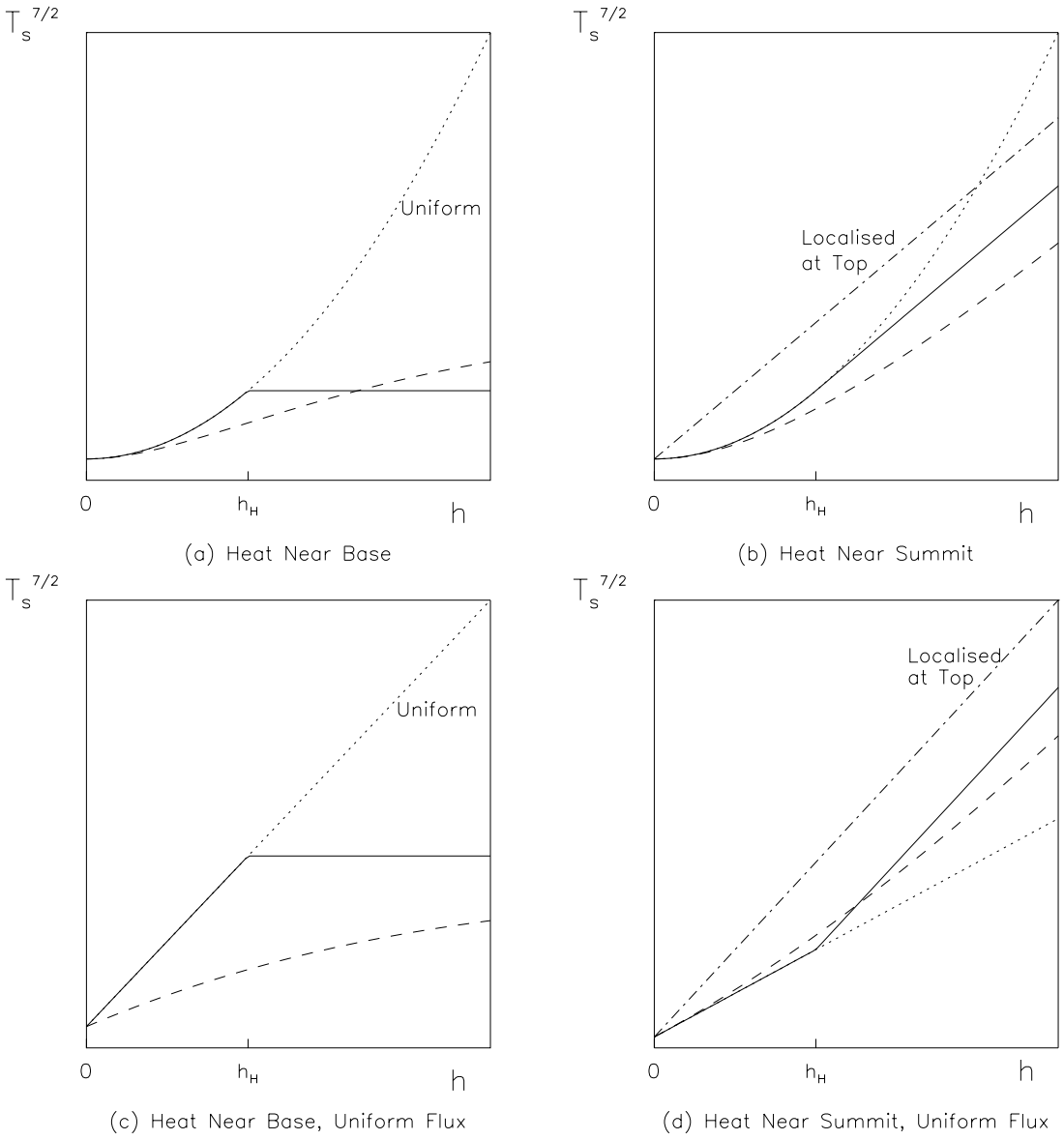

FIG. 4.—Summit temperatures (T_s) of loops in a coronal arcade as a function of height (h) (*a*) when the heating is the same per unit volume at the top of each loop and within each loop the heating is uniform (*dotted line*), uniform up to a distance L_H from the base (*solid line*), or of the form $H = H_0 \exp(-s/L_H)$ (*dashed line*); (*b*) when the heating is the same per unit volume at the top of each loop and is uniform within each loop down to a distance L_H from the summit (*solid line*), concentrated at the summit (*dot-dashed line*), or of the form $H = H_0 \exp[(s - L)/L_H]$ (*dashed line*). When the heat flux at the base is the same on all loops, the profiles are shown in (*c*) for a heating that is uniform (*dotted line*), truncated at a distance L_H from the base (*solid line*) or exponentially decaying (*dashed line*) and in (*d*) for heating truncated at a distance L_H from the summit (*solid line*), concentrated at the summit (*dot-dashed line*) and exponentially decaying from the summit as $H_0 \exp(-s/L)$ (*dashed line*).

arcade (Fig. 5*c*), so that each loop profile is of the form of equation (2.13) when $L > L_H$ or equation (2.7) when $L < L_H$. The arcade profile then becomes

$$T_s = \begin{cases} T_0(1 + c_H h^2/R_\odot^2)^{2/7}, & h < h_H, \\ T_0[1 + c_H h_H(2h - h_H)/R_\odot^2]^{2/7}, & h > h_H, \end{cases} \quad (3.6)$$

for a uniform-heat arcade and

$$T_s = \begin{cases} T_0(1 + hc_F/R_\odot)^{2/7}, & h < h_H, \\ T_0[1 + c_F(2h - h_H)/R_\odot]^{2/7}, & h > h_H, \end{cases} \quad (3.7)$$

for a uniform-flux arcade, as shown by solid curves in Figures 4*c* and 4*d*, respectively. Again, $h_H = 2L_H/\pi$ is the height in the arcade below which there is uniform heating. Thus the characteristic effect of such heating for a uniform-heat arcade is to make $T_s^{7/2}$ increase quadratically at low heights and linearly at large heights. For a uniform-flux arcade it increases linearly at low heights and linearly at large heights but with twice the gradient.

Fourth, the particular case when the heating is localized at the summit of each loop (Fig. 5*d*) gives the summit temperature for each loop as equation (2.16). The resulting arcade profile is

$$T_s = T_0(1 + 2C_H h/R_\odot^2)^{2/7} \quad (3.8)$$

for a uniform-heat arcade as graphed in Figure 4*c* (*dot-dashed curve*) where $C_H = 7f_0 R_0^2 \pi/(8\kappa_0 T_0^{7/2})$. The corresponding profile for a uniform flux arcade (Fig. 4*d*, *dot-dashed curve*) is

$$T_s = T_0(1 + 2c_F h/R_\odot)^{2/7}. \quad (3.9)$$

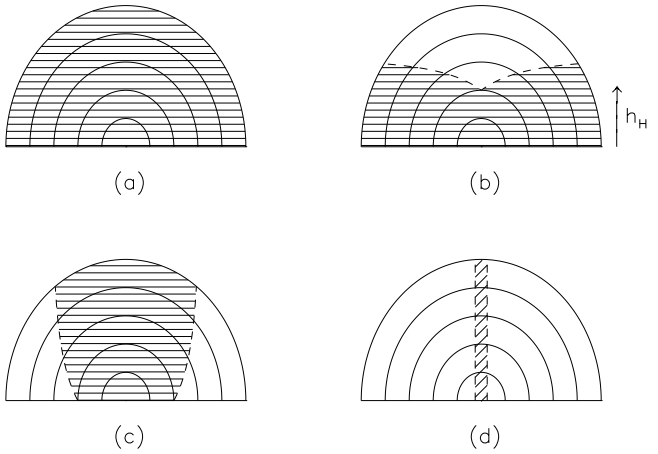

FIG. 5.—Location (*shaded*) of the heating region in the arcade for (*a*) uniform heating, (*b*) heating near the base of each loop, (*c*) heating near the loop summits, and (*d*) heating localized at the summits.

Thus we find that in this case $T_S^{7/2}$ increases linearly with height for both a uniform-heat and a uniform-flux arcade. Other semicircular arcade models are discussed in Appendix B.

3.2. *Line-Current Arcade*

So far we have considered a heating that is independent of magnetic field strength and an arcade of semicircular field lines, but both of these assumptions may be easily relaxed to produce more general models. For example, consider first the potential arcade with circular field lines and a magnetic field that is constant on each field line with magnitude

$$B_\phi = \frac{B_d d}{r} \tag{3.10}$$

because of a line current submerged a distance d, say, below the coronal base and giving a value B_d at distance $r = d$ (Fig. 6*a*). A field line that extends to a summit height h has a footpoint with coordinates (r_0, θ_0), where $r_0 = d + h$. The length of such a field line from footpoint to summit is therefore $L = (\frac{1}{2}\pi - \theta_0)r_0$, where $r_0 \sin\theta_0 = d$, or, in other words,

$$L(h) = (d + h)\cos^{-1}\frac{d}{d+h}\,. \tag{3.11}$$

At low heights it increases like $h^{1/2}$ and at large heights like h (Fig. 6*b*).

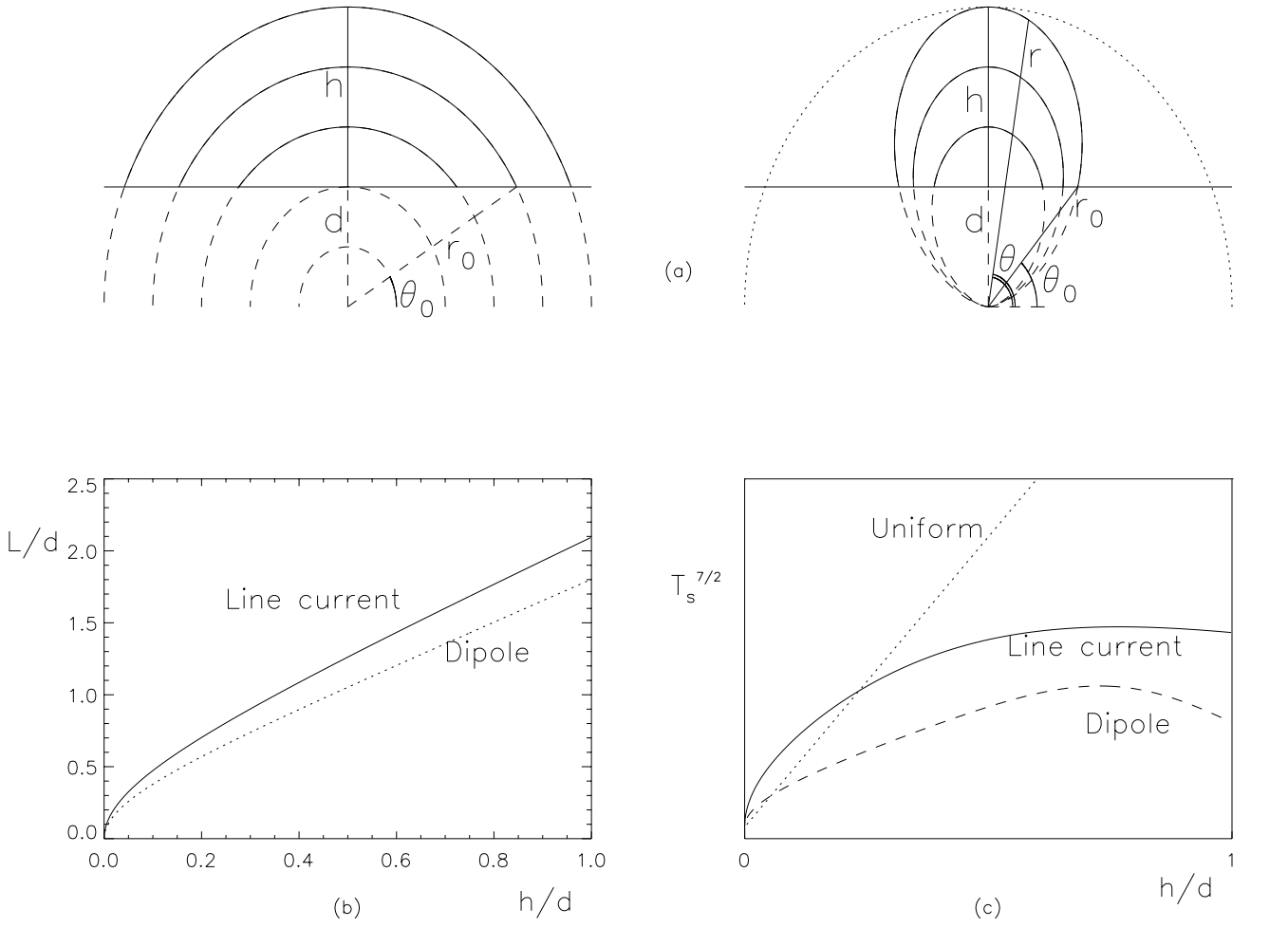

FIG. 6.—(*a*) Notation for the field due to a line current or a dipole at depth d, whose field lines have summit height h and footpoint coordinates (r_0, θ_0). (*b*) Variation of the length (L) of a field line with its summit height (h). (*c*) Summit temperature (T_s) as a function of height (h) for heating that is uniform or proportional to the square of the magnetic field due to a line current or a dipole.

If the heating is uniform along each field line with, say, the same base heating flux for each loop, the semicircular arcade temperature (eq. [3.3]) is replaced by

$$T_s = T_0\left[1 + \frac{2c_F}{\pi}\frac{L(h)}{R_\odot}\right]^{2/7}, \quad (3.12)$$

where the function $L(h)$ is given by equation (3.11). Suppose now that each loop is uniformly heated along its length and the heating flux at its base scales as the square of the magnetic field at the base. For a loop with a summit at an altitude h, the base field is, according to equation (3.10), $B_o = B_d d/(d + h)$ and the summit temperature (eq. [3.12]) becomes

$$T_s = T_0\left[1 + \frac{2c_{F0}}{\pi(1 + h/d)^2}\frac{L(h)}{R_\odot}\right]^{2/7}, \quad (3.13)$$

where the heating constant (c_{F0}) defined below equation (3.3) is evaluated at the arcade base. The resulting temperature profiles are shown in Figure 6*c*.

If we assume on the other hand that the volumetric heating rate scales as the square of the local magnetic field, the summit temperature becomes

$$T_s = T_0\left[1 + \frac{4c_{H0}}{pi^2(1 + h/d)^2}\frac{L^2(h)}{R_\odot^2}\right]^{2/7}, \quad (3.14)$$

where c_{H0} defined below equation (3.2) is evaluated at the arcade base.

The corresponding results for a dipole arcade are given in Appendix C.

4. *YOHKOH* OBSERVATIONS OF LOOPS AND ARCADES

Weak soft X-ray emission has been observed with *Yohkoh* from large closed regions that extend up to 0.8 $R_\odot$ above the limb and evolve slowly over long periods of time. Magnetic field extrapolations demonstrate that the largely structureless emission arises in large-scale magnetically closed regions and almost always underlies coronal streamers (Acton 1996). The visibility of specific loops in an X-ray image depends on the temperature and density contrast along neighboring magnetic flux tubes. Low-altitude, intensely heated loops are easily distinguished (Fig. 7*a*). At large heights, entire loops may be seen (*top left* and *top right* of Fig. 7*a*), but often only the parts near the base are indentifiable, arching round with a convex curvature toward the solar limb (*bottom right* of Fig. 7*a*). We have analyzed in detail the loop that is outlined in the top right of Figure 7*a* and clearly shown in close-up in Figure 7*b*.

We carefully corrected the Soft X-Ray Telescope images for the effect of radiation scattered from other areas of the Sun because of the broad low-level wings of the telescope point-spread function (Foley et al. 2000). The level of the scattered signal amounts to about 5% of the observed flux at the loop footpoints and 20% at the loop top (Foley 1998). Temperatures were obtained by the filter ratio technique (Tsuneta et al. 1991) for a single diffuse region. The data were aligned to within 2″ and corrected for the effects of CCD saturation, dark noise, and particle hits. For example, Figures 7–10 show a global image of the Sun on 1992 October 3, and the resulting temperature variation along the length of a loop and with height at the symmetry axis of an arcade. The temperature in such arcades rises rapidly and levels off at typically 2.2–2.3 MK at an altitude of 1.5 $R_\odot$, but according to Culhane (1997) and Kano & Tsuneta (1996), the individual loops do not obey the usual scaling law, namely, that $T \sim (pL)^{1/3}$ (Rosner, Tucker, & Vaiana 1978). In any case it is the shape of the temperature profile that matters for the present analysis rather than the absolute temperature values, since a global increase or decrease of temperature would not change the shape of the profile.

4.1. *Errors*

The errors in the temperature reflect the statistical uncertainty in the data as were presented by Sturrock et al. (1996). The only departure from their work in our error analysis is that a minimum count rate was used to determine the size of each bin along the loop. The errors within the bin were summed in quadrature. The uncertainties in the temperatures were determined as described in Klimchuck & Gary (1995).

A discussion of systematic errors associated with the overall telescope calibration is included in Klimchuck & Gary (1995) and Porter & Klimchuck (1995). These, although estimated to be less than 2% of the intensity calibration, were shown to be capable of introducing an uncertainty into the temperatures determined here of the order 0.8 MK. However, the analysis that we perform is dependent upon the profile of the temperature rather than the absolute values of the temperature. Another source of systematic uncertainty in these data is that associated with telescope scattered light. This can become important for temperature profiles obtained in the high corona since its relative contribution increases with distance off axis. The possible effect of this uncertainty has been minimized by a careful examination of the scattering characteristics observed within the SXT images of solar flares.

4.2. *Loop Analysis*

To try to determine which form of heating best fits the data, we analyzed three sets of observations of different quiet coronal loops and compared them with different models of heat deposition. The first data set is for the loop shown in Figure 7 on the right limb. The second data set is for the loop on the left limb in Figure 7, and the third set is for a loop observed in the northern hemisphere on the 1992 June 3. For the first and third data sets the entire temperature profile from footpoint to footpoint is compared with the models, but for the second data set only half of the loop is compared since an active region lying to the southern end of the loop contaminates the data for the other half of the loop.

The temperature variation for the first data set at 10 points is shown in Figure 8. It increases from 1.6 MK at one coronal footpoint up to about 2.2 MK at the summit and then falls to about 1.6 MK at the other footpoint. This type of temperature profile is typical of all three data sets. We have compared the observed temperature profiles with the models of § 2 that have main steady state balance between the dominant effects at these temperatures, namely, thermal conduction and a heating that is assumed to depend only on the distance along the loop. In doing so, for simplicity we assume the observed structure is a loop in a plane perpendicular to the line of sight and ignore projection effects that should be incorporated in a more complete analysis. [If the loop were inclined such that an element ds made a known angle $\phi(s)$ with the plane of the sky, then our basic equation would still hold but with the cross section $A(s)$ changed by a

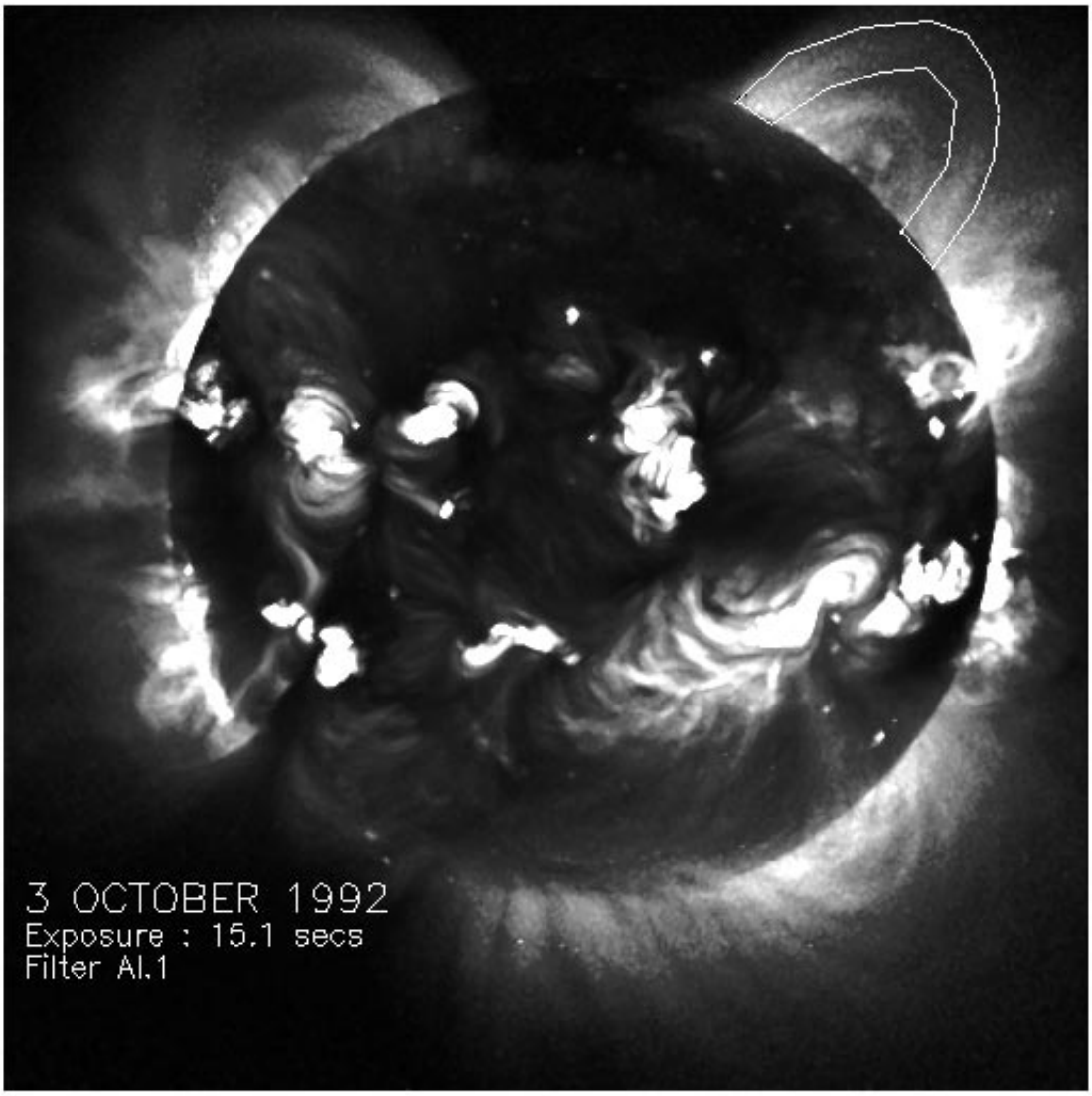

FIG. 7a

FIG. 7.—Soft X-ray images of the Sun on 1992 October 3 showing a loop on the right limb that we have analyzed in detail (*a*) outlined on a global image and (*b*) in a close-up of the region.

factor cos $\phi(s)$ and the heating $H(s)$ changed by a factor $\sec^2 \phi(s)$.] The effects of radiation on the temperature profiles are negligible at these temperatures: here radiation is typically 10–100 times smaller than conduction in the energy balance (depending on the density), which therefore determines the temperature independently of the pressure and density; gravity makes the pressure and density fall off with height but does not influence the temperature profile. In the comparison, a variety of forms for the heating is adopted. For each model the most likely values of the parameters have been determined by a weighted least-squares analysis, minimizing

$$\lambda = \sum_i \frac{[T_{\rm obs}(s_i) - T_{\rm mod}(s_i)]^2}{\sigma_i^2}, \qquad (4.1)$$

where σ_i is the width of the error bar in the measured temperature ($T_{\rm obs}$) at distance s_i (or altitude h_i) and $T_{\rm mod}$ is the corresponding model temperature. In theory, a better statistical measurement of the minimization would be to use a χ^2 analysis, in which σ_i would be the standard deviation of $T_{\rm obs}$ at s_i. To calculate σ_i at each point, one would require a distribution of $T_{\rm obs}$, which is not available in the present data, so we adopt a simpler approach and normalize each term in the fit with respect to the width of the error bar. Dividing by the number (n) of degrees of freedom gives a quantity (λ/n) such that the lower the value of this parameter relative to other fits the better is the comparison between the observed and model temperatures for a given value of n. The absolute values of λ/n have no rigorous meaning, but the relative values for a given n enable one to say which fit is better.

First of all, the data for the loop shown in Figure 7*b* have been compared with three different heating models. The first one has a given base temperature (T_0) and a maximum in its heating rate (H_0) per unit volume at the loop base; it decays exponentially along the loop over a distance $L_H = 0.1L$, where L is the loop half-length, so that the temperature profile is given by equation (A3). Minimization with respect to the parameters T_0 and H_0 yielded a very poor fit for the temperature profile (Fig. 8*a*) with a λ/n of 5.4. The second model has a heat source concentrated at the loop summit and a temperature profile given by equation

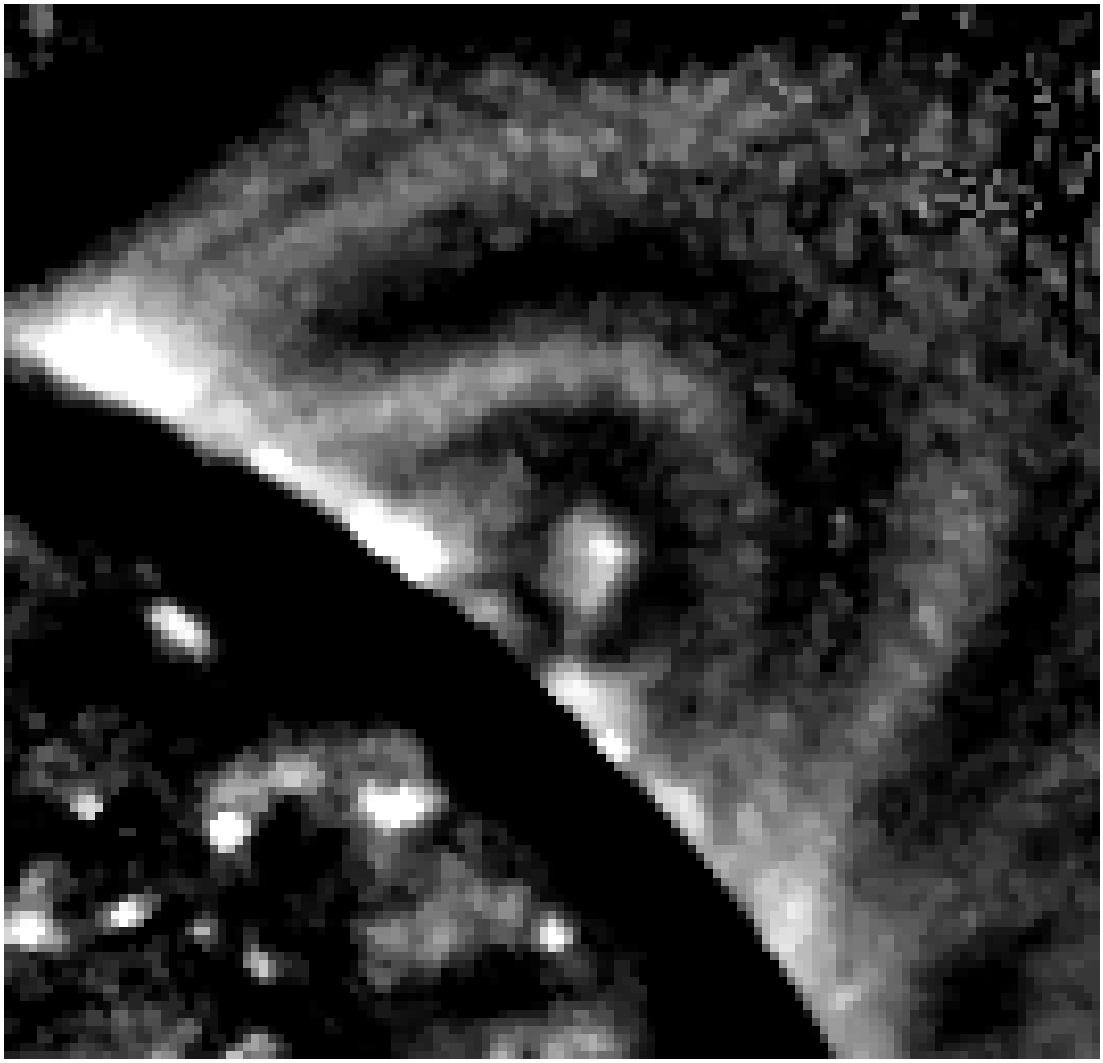

FIG. 7*b*

(2.15). It gives a better fit (Fig. 8*b*) since the resulting value of λ/n (namely, 1.7) is smaller.

The third model has uniform heating (H_0) and a temperature profile given by equation (2.5). The resulting minimization gave a rather good fit with a λ/n of 0.89 (Fig. 8*c*). The corresponding values of T_0 and $\overline{H}$ are 1.61 MK and 3.75, respectively. The latter gives a dimensional value of H_0 of 1.09×10^{-6} J m^{-3} s^{-1}, so for a loop half-length (L) of 700 Mm this produces a base energy flux of

$$|F(0)| = H_0 L = 760 \text{ J m}^{-2} \text{ s}^{-1}$$
$$= 7.6 \times 10^5 \text{ ergs cm}^{-2} \text{ s}^{-1} .$$

Finally, we repeated the procedure with equation (2.9) but with L_H as an extra parameter. Normally, one would expect an extra such degree of freedom to lead to a better fit, but in this case the λ/n was found to be virtually the same as for the uniform heating case. The profile (Fig. 8*d*) was almost the same and L_H was $20L$ and so much larger than the loop length.

We chose to study the temperature of the first loop at 10 points in order to reduce the measurement uncertainties as much as possible while retaining a significant number of points along the loop. For comparison, the corresponding results for 74 points are shown in Figure 9. Here the error with each point is much greater but the qualitative conclusions are the same. The λ/n values for each of the graphs are (Fig. 9*a*) 0.71, (Fig. 9*b*) 0.5, (Fig. 9*c*) 0.35, and (Fig. 9*d*) 0.4. Therefore, uniform heating again gives the lowest value, with T_0 and $\overline{H}$ equal to 1.62 MK and 3.51, respectively, which are close to the previous values. It should be noted here that as the number of points is increased from 10 to 74 the value of the minimization parameter decreases. All of the values of (λ/n) for 74 data points are less than those for 10 points since many more points are compared. However, again uniform heating gives the best relative fit. The values of λ/n and an eye fit suggest that there is no real difference in the fit of the models in Figs. 9*b* and 9*d*, but the model (Fig. 9*c*) of uniform heating certainly gives a better fit by eye. The analysis certainly cannot rule out the models in Figs. 9*b* and 9*d*, and an explicit calculation of probability or statistical significance is not possible since this is a weighted least-squares method rather than a χ^2 method. Nevertheless, the above comparison provides strong evidence against heating concentrated near the loop base and suggests that heating uniformly distributed along the loop is more likely than heating concentrated at the summit.

In Figure 8*c* the theoretical curve does not pass through the error bars of three of the points. However, if the sta-

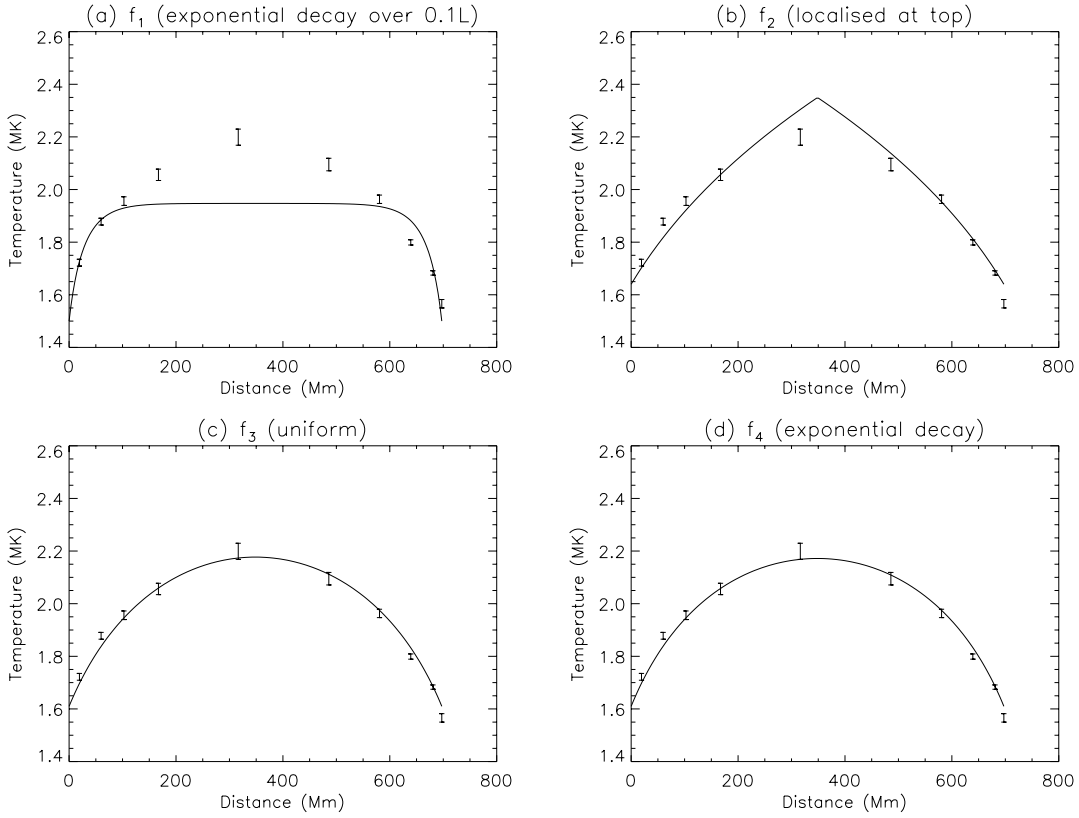

FIG. 8.—First data set. Observed temperature in MK as a function of distance at 10 points along the loop on the right limb of Fig. 7*a* with the errors shown. Also included are the best fit model temperatures for heating that is (*a*) decaying from the feet over a tenth of the loop length, (*b*) concentrated at the summit, (*c*) uniform, and (*d*) decaying from the feet over a distance L_H.

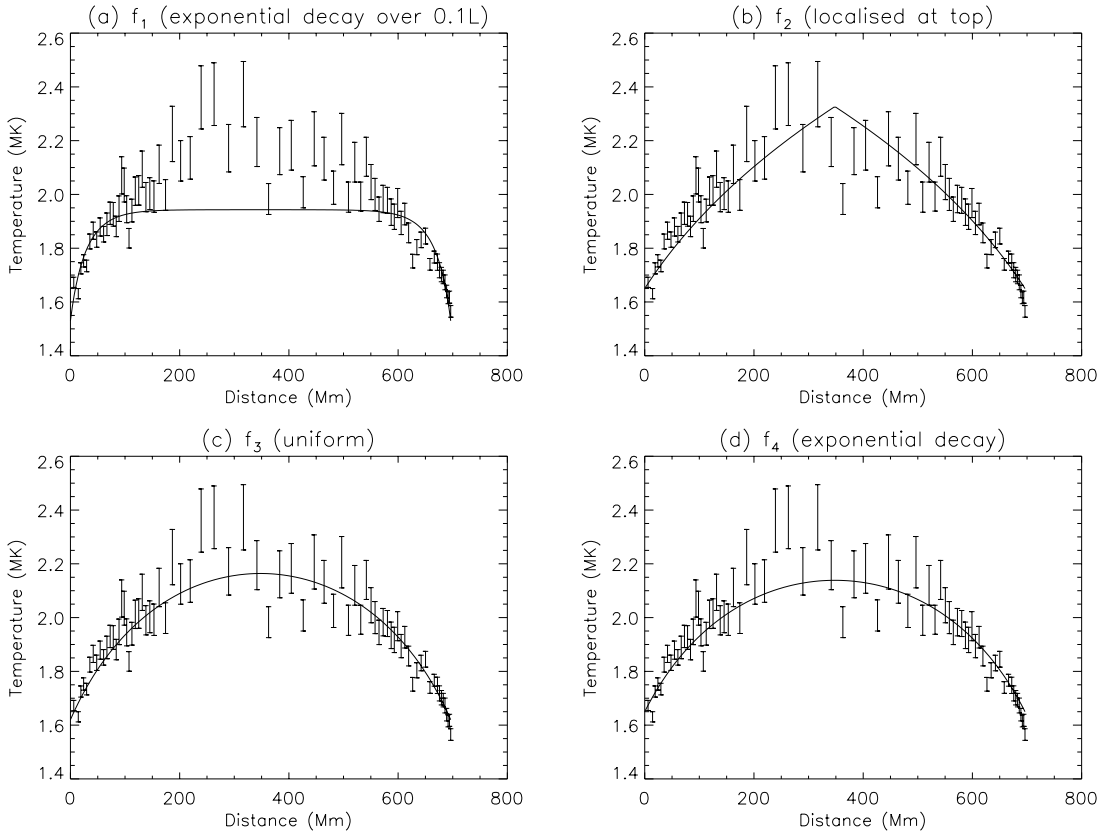

FIG. 9.—Same as Fig. 8 but with temperature measured at 74 points along the loop

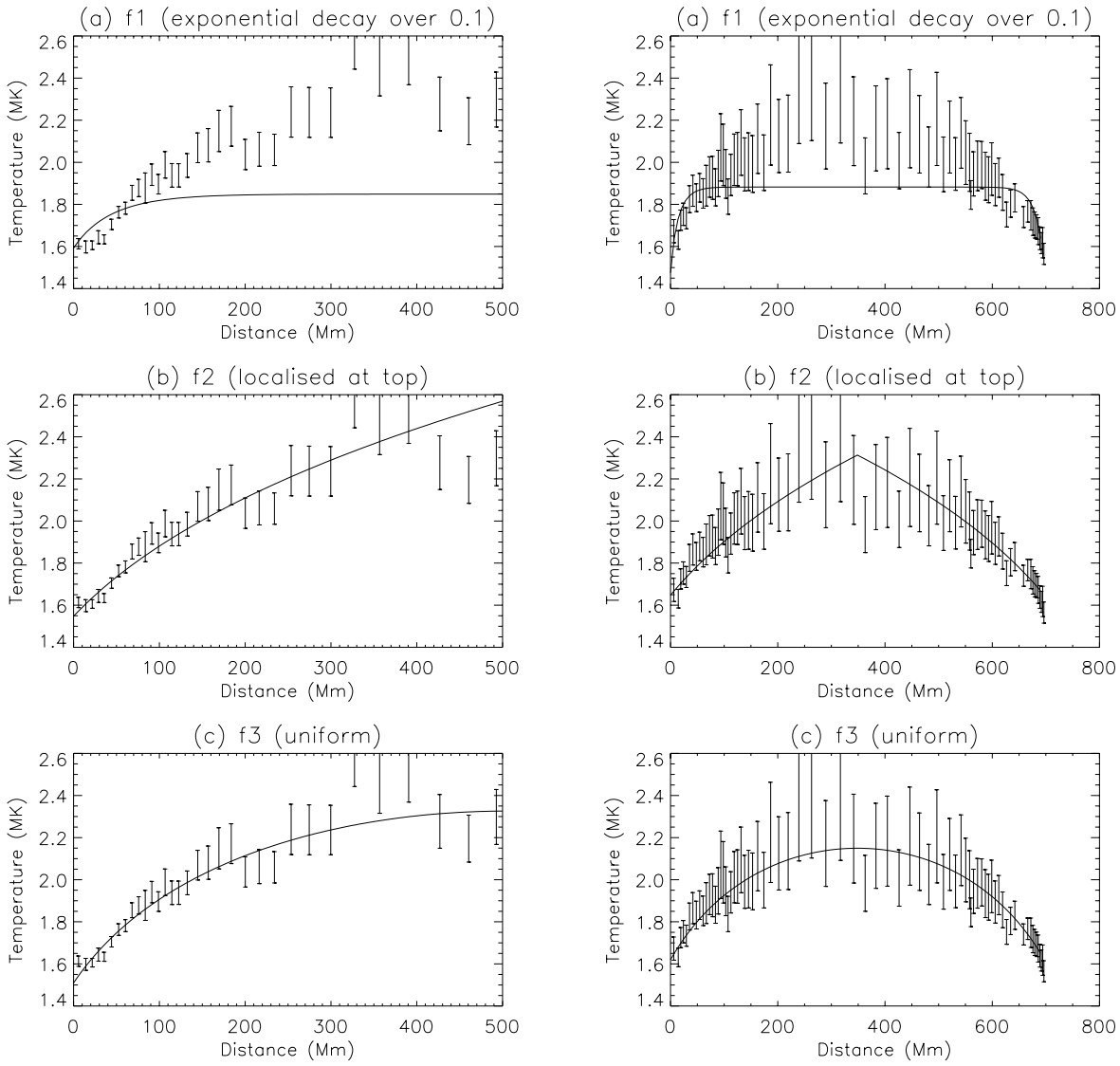

FIG. 10.—Results for the second data set on the left (from the loop on the left limb of Fig. 7*a*) and for the third data set on the right (from a loop on 1992 June 3).

tistical error bars are increased by only 60% to include systematic errors such as contamination along the line of sight, the curve passes through all the points and uniform heating remains a much better fit than heating concentrated near the footpoints.

From the analysis it can be seen that the temperature profile along the quiet coronal loop seen on the right of Figure 7*a* is more likely to be produced by uniform heating than the three others forms considered. The fitting procedure was next repeated for the second and third data sets. For the second data set 33 points along half of the loop on the left limb of Figure 7*a* were compared with the models and for the third data set 74 points along the whole loop length were used. The results can be seen in Figure 10. The fits are shown for (Fig. 10*a*) heat decaying exponentially from the base ($L_H = 0.1L$), (Fig. 10*b*) heat localized at the top, and (Fig. 10*c*) uniform heating. For the second data set it can be clearly seen that uniform heating again produces the best fit with a λ/n value of 0.35 ($T_0 = 1.51$, $H_0 = 8.55$) compared to a λ/n of 2.6 for heat decaying from the base and 0.47 for heat localized at the summit. For the third data set uniform heating gives a λ/n value of 1.23 ($T_0 = 1.76$, $H_0 = 2.64$) compared to 1.41 for exponential decay from the base and 1.42 for heat localized at the top. Even though these values lie closer together than the other data sets, uniform heating still produces the best fit, as a visual inspection of Figure 10 would suggest. For all three data sets, therefore, uniform heating along the loop is more likely to produce the observed temperature profiles than heat decaying from the footpoints or heat localized at the top.

4.3. *Arcade Analysis*

The loop outlined in Figure 7 represents the outermost loop of a beautiful arcade of loops arching high above the solar surface, so we decided to measure the temperature at the summits of the loops as a function of height, as shown in Figure 11. Again we neglect projection effects and assume we are observing a nested set of loops one above the other in a plane perpendicular to the line of sight.

We first considered the model given by equation (3.2) in which the heating is deposited uniformly throughout the whole arcade, so that the heating flux on each loop is pro-

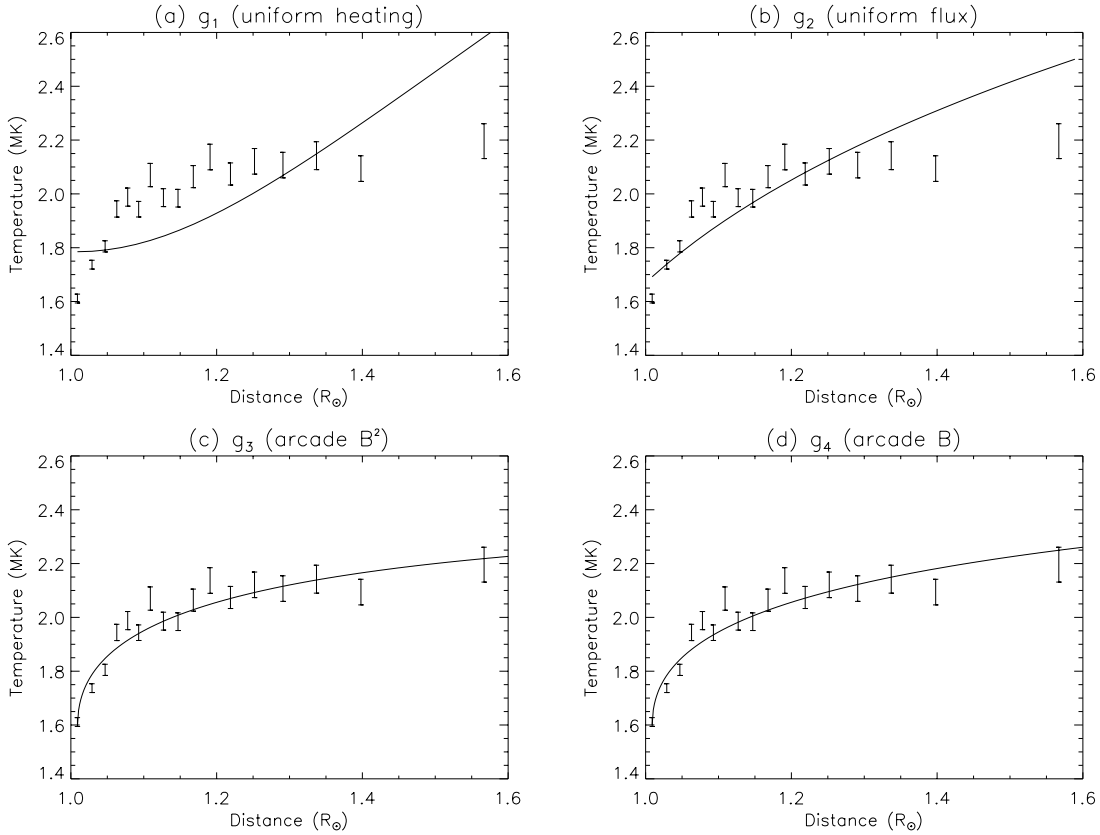

FIG. 11.—Observed temperature as a function of height at the summits of the loops that comprise the arcade whose outermost loop is indicated in Fig. 6*a*. The temperature (in MK) is shown as a function of distance from the solar center (in units of 1 $R_\odot$ = 700 Mm) for models with a uniform heating on each loop but with a flux that is (*a*) proportional to loop length, (*b*) uniform, (*c*) proportional to the square of the arcade magnetic field, and (*d*) proportional to the arcade magnetic field.

portional to loop length and found a poor fit (Fig. 11*a*) with a λ/n of 4.95. Next, we assumed instead the same heating flux on each loop and so found the best-fitting model of the form of equation (3.3). This gave a better fit with a λ/n of 1.83 (Fig. 11*b*). It is consistent with a model in which a Poynting flux feeds energy upward from the solar surface into coronal loops.

Many coronal heating models depend on the strength of the magnetic field in some way, which in turn decreases with altitude. We also therefore considered a heating flux that is proportional to the square of the magnetic field strength, which in turn we assumed for simplicity to be due to a potential field from a line current of depth d, say, below the coronal base. Such a model arcade is a reasonable representation of the observed structure and gives a series of loops that are arcs of circles and have constant cross sections with the field strength falling off inversely with distance from the axis below the solar surface. Comparing the observations with the resulting temperature profile [eq. (3.13) with $L(h)$ given by eq. (3.11)] and minimizing with respect to $\overline{H}$ and d then gave an excellent fit (Fig. 11*c*) and a λ/n of 0.49. For comparison, we also considered a flux proportional to the magnetic field (rather than its square), which also gave a good fit (Fig. 11*d*) with a λ/n of 0.51, so we have little ability to discriminate at present about what power of the magnetic field is important.

The comparison with the arcade observations therefore gives extra information about the form of the heating mechanism in addition to what we deduced from the loop observations. In particular, there seems to be good evidence in favor of the heating flux being the same from one loop to another rather than the heating being deposited uniformly throughout the arcade. In addition, the model with the heating being proportional to the square of the magnetic field strength (assumed to have circular field lines) rather than being uniform appears to be favored.

5. TEMPERATURE PROFILE IN CORONAL HOLES

We now address the question of the temperature profile low down in a coronal hole in the same spirit as we dealt with the temperature profiles in loops. With the *Yohkoh* SXT instrument Foley et al. (1997) have produced some measurements of such profiles that deserve analysis, even though they are of a lower quality (because the X-ray flux is smaller) than those obtained for arcades of loops.

Coronal hole measurements give us the profile with height of the plasma temperature. As before, we can compare the effects of various possible distributions of the volumetric heating rate with these data. Since the quality of the data is somewhat less than those for closed loops we shall discuss only simple (one-fluid) models for the heating and for the field line geometry. The starting point is again equation (3.1), where we moreover assume for simplicity that the magnetic field lines are radial and straight. The position variable is taken as the distance r from the center of the Sun. Then equation (3.1) assumes the simpler form

$$\frac{\kappa_0}{r^2}\frac{d}{dr}r^2T^{5/2}\frac{dT}{dr} = -H(r) \qquad (5.1)$$

and integrates to

$$\kappa_0 T^{5/2} \frac{dT}{dr} = F_0 \frac{R_\odot^2}{r^2} - \frac{1}{r^2} \int_{R_\odot}^{r} r'^2 H(r') dr' , \qquad (5.2)$$

where the integration constant (F_0) represents the absolute value of the heat flux at the base, at $r = R_\odot$. The boundary conditions that apply to the differential equation (5.1) differ from those that apply in magnetically closed regions, since heat can now leak to infinity. We shall assume that the temperature (T_0) at the base is known as well as the temperature (T_∞) at infinity. The value that should be selected for the latter, however, cannot be precisely defined, since the purely conductive energy equation loses validity when one moves from the solar corona to the solar wind region proper. Choosing an appropriate value for this quantity will then be a rough way of representing the heat conduction and advection physics that takes place at distances from the Sun approaching or exceeding the distance of the sonic critical point, namely, about 5 $R_\odot$. The heat conduction equation is a good representation of energy transport at distances less than this and, in particular, at those distances where the measurements have been made.

Integrating equation (5.2) once more gives the temperature profile as

$$\frac{2\kappa_0}{7} T^{7/2} = \frac{2\kappa_0}{7} T_0^{7/2} + \int_{R_\odot}^{r} \frac{dr'}{r'^2} \times \left[F_0 R_\odot^2 - \int_{R_\odot}^{r'} r''^2 H(r'') dr'' \right] . \qquad (5.3)$$

This solution satisfies the boundary condition at the base, and the flux integration constant (F_0) can be chosen such that the boundary condition at infinity be satisfied too. This gives

$$F_0 R_\odot = \int_{R_\odot}^{\infty} \frac{dr'}{r'^2} \int_{R_\odot}^{r'} r''^2 H(r'') dr'' - \frac{2\kappa_0}{7} (T_0^{7/2} - T_\infty^{7/2}) , \qquad (5.4)$$

and finally the temperature is given as a function of r by

$$\frac{2\kappa_0}{7} T^{7/2} = \frac{2\kappa_0}{7} T_\infty^{7/2} + \frac{2\kappa_0}{7} (T_0^{7/2} - T_\infty^{7/2}) \frac{R_\odot}{r} + \int_{r}^{\infty} \frac{dr'}{r'^2} \int_{R_\odot}^{r'} r''^2 H(r'') dr'' - \frac{R_\odot}{r} \int_{R_\odot}^{\infty} \frac{dr'}{r'^2} \int_{R_\odot}^{r'} r''^2 H(r'') dr'' . \qquad (5.5)$$

This general expression is valid for any profile of the heating rate $H(r)$. It is interesting to discuss whether the resulting temperature profile has an extremum or decreases continuously from the base to infinity. From equation (5.2) above for the heat flux, the temperature maximum, if it exists, will be situated at a radius ($\bar{r}$), which is a solution of the equation

$$F_0 R_\odot^2 = \int_{R_\odot}^{\bar{r}} r'^2 H(r') dr' . \qquad (5.6)$$

Let us now take into account equation (5.4) between the base flux (F_0) and the temperature at infinity (T_∞) and also define a function $G(r) = \int_{R_\odot}^{r} r'^2 H(r') dr'$, which increases from 0 at $r = R_\odot$ to a value G_∞ at infinity. Then equation (5.6) can be restated as an equation for the value ($\bar{G}$) of G at the temperature maximum, namely,

$$\int_{R_\odot}^{\infty} \frac{dr' R_\odot G(r')}{r'^2} - \frac{2\kappa_0 R_\odot}{7} (T_0^{7/2} - T_\infty^{7/2}) = \bar{G} . \qquad (5.7)$$

The integral on the left-hand side is smaller than G_∞, and the equation for the position ($\bar{r}$) of the temperature maximum has a solution if the left-hand side is positive, which implies that T_0 be not too large; otherwise, $T(r)$ decreases monotonically from the base to infinity.

To be specific, assume that the function $r^2 H(r)$ is a step function, so that the heating is limited to some region at the base of the corona between $R_\odot$ and $R_\odot + L$. In other words, we assume that for r between $R_\odot$ and $R_\odot + L$, $r^2 H(r) = H_0 L^2$, where H_0 is a constant, whereas for larger values of r it vanishes. Such a heating profile gives an integrated heating rate that is constant per unit length along conical flux tubes up to some limiting height L. The corresponding function $G(r)$ is linear between $R_\odot$ and $R_\odot + L$ and constant for larger r's. After some algebra and using equation (5.4) to express F_0 in terms of T_∞, we obtain the temperature profile in the following form:

$$\frac{2}{7} \kappa_0 T^{7/2}(r) = \frac{2}{7} \kappa_0 \left[T_\infty^{7/2} + (T_0^{7/2} - T_\infty^{7/2}) \frac{R_\odot}{r} \right] + H_0 L^2 \times \left[1 + \left(1 - \frac{R_\odot}{r} \right) \log \left(\frac{R_\odot + L}{R_\odot} \right) - \frac{R_\odot}{r} + \log \left(\frac{R_\odot}{r} \right) \right] , \quad \text{if } R_\odot \le r \le R_\odot + L , \qquad (5.8)$$

and

$$\frac{2}{7} \kappa_0 T^{7/2}(r) = \frac{2}{7} \kappa_0 \left[T_\infty^{7/2} + (T_0^{7/2} - T_\infty^{7/2}) \frac{R_\odot}{r} \right] + \frac{H_0 L^2 R_\odot}{r} \left[\frac{L}{R_\odot} - \log \left(1 + \frac{L}{R_\odot} \right) \right] , \quad \text{if } r \ge R_\odot + L .$$

Such a function decreases as $1/r$ for large r, and, if the base temperature is small enough to allow the temperature profile to reach a maximum, it is reached at a value ($\bar{r}$) of r that is less than ($R_\odot + L$), namely, at

$$\bar{r} = R_\odot \left(1 + \frac{F_0 R_\odot}{H_0 L^2} \right) . \qquad (5.9)$$

This may be written in terms of T_∞ as

$$\bar{r} = (R_\odot + L) - R_\odot \left[\frac{L}{R_\odot} - \log \left(1 + \frac{L}{R_\odot} \right) \right] - \frac{2}{7} \frac{\kappa_0 R_\odot}{H_0 L^2} (T_0^{7/2} - T_\infty^{7/2}) , \qquad (5.10)$$

which is indeed smaller than $R_\odot + L$ because the last two terms on the right-hand side are negative. The value of $\bar{r}$ is also larger than $R_\odot$ if T_0 is not too large. The temperature

($\overline{T}$) at the maximum is given by

$$\frac{2}{7}\kappa_0 \overline{T}^{7/2} = \frac{2}{7}\kappa_0 T_0^{7/2} + H_0 L^2 \times \left[\frac{F_0 R_\odot}{H_0 L^2} - \log\left(1 + \frac{F_0 R_\odot}{H_0 L^2}\right)\right]. \quad (5.11)$$

The observational data reported in the paper by Foley et al. (1997) are not very precise. They report a maximum temperature in coronal holes of 1.5 MK at 1.4 $R_\odot$, which was found by Ko et al. (1997) from ion populations recorded in the solar wind with *Ulysses* SWICS. Foley et al. (1997) found a temperature at the base of 1.1 MK and at 1.15 $R_\odot$ of 1.35 MK. The base value, however, does not accurately represent the temperatures close to the coronal base because temperatures below 1 MK are effectively veiled by the hotter coronal hole material (originating from greater heights) that lies along the same line of sight. A better value at the coronal base would be 0.5 MK (Withbroe 1988). For our purposes, we shall therefore adopt a base temperature (T_0) of approximately 0.5 MK and a temperature maximum of 1.5 MK reached at approximately 1.4–1.5 $R_\odot$. The data give no clue about a reasonable value of the temperature at infinity, which we shall assume, by default, to vanish. We do need, however, to determine the parameters F_0, H_0 and L. Gathering the results obtained above, and introducing the convenient dimensionless variables

$$r^* = \frac{\bar{r}}{R_\odot}, \quad F_0^* = \frac{F_0 R_\odot}{H_0 L^2}, \quad T^* = \frac{\overline{T}}{10^6 \text{ K}}, \quad T_0^* = \frac{T_0}{10^6 \text{ K}},$$

the position (eq. [5.9]) of the temperature maximum gives the equation

$$r^* = 1 + F_0^*, \quad (5.12)$$

the value of the temperature maximum (eq. [5.11]) gives the equation

$$T^{*7/2} - T_0^{*7/2} = \frac{7 H_0 L^2}{2 \times 10^{21} \kappa_0}\left[F_0^* - \log(1 + F_0^*)\right], \quad (5.13)$$

and the relation between the flux and the heating rate (eq. [5.4]) gives, with $T_\infty = 0$,

$$F_0^* = \log\left(1 + \frac{L}{R_\odot}\right) - \frac{2 \times 10^{21}\kappa_0}{7 H_0 L^2} T_0^{*7/2}. \quad (5.14)$$

The observed data suggest, with large uncertainties, that $T^* = 1.5$, $r^* = 1.5$, and $T_0^* = 0.5$. The value of κ_0 is 9.24×10^{-12} J m^{-1} s^{-1} for a Coulomb logarithm of 20. We adopt $r^* = 1.5$ as the position of the temperature maximum so that $F_0^* = 0.5$. From the equations (5.13) and (5.14) we then find

$$\log\left(1 + \frac{L}{R_\odot}\right) = F_0^* + T_0^{*7/2}\frac{F_0^* - \log(1 + F_0^*)}{T^{*7/2} - T_0^{*7/2}},$$

which gives

$$\frac{L}{R_\odot} = 0.65.$$

We finally obtain $H_0 L^2$ from equation (5.13) and from it the absolute value of the base flux (in MKSA units), namely, $F_0 = F_0^* H_0 L^2 / R_\odot$. We can deduce then a value for the heating flux, i.e., $F_0 \approx 1.6 \times 10^5$ ergs cm^{-2} s^{-1}.

However, the data do have large uncertainties. Changing the position of the temperature maximum to $r^* = 1.4$ gives $L/R_\odot = 0.40$ and $F_0 \approx 1.93 \times 10^5$ ergs cm^{-2} s^{-1}. Changing the temperature at the base to 1.0 MK still with $r^* = 1.5$ and $T^* = 1.5$ gives $L/R_\odot = 0.70$ and $F_0 = 1.87 \times 10^5$ ergs cm^{-2} s^{-1}. A much lower position of the temperature maximum, which seems also to be consistent with the quoted data, at, say, $r^* = 1.15$ with the maximum temperature of $T^* = 1.35$, still with $T_0^* = 0.5$ gives $L/R_\odot = 0.17$ and $F_0 = 3.1 \times 10^5$ ergs cm^{-2} s^{-1}. That the flux so obtained is rather small in the case of a high-altitude location of the temperature maximum can be understood, because it represents only that part of the flux that is associated with the conductive losses of the low corona back to the solar surface, and these are lower for a less steep temperature increase. Moreover, assuming the temperature to reach an asymptotic value at infinity in a purely conductive model is equivalent to neglecting the enthalpy and kinetic energy losses of the solar wind. A realistic estimate of the energy flux entering the corona at the base of polar coronal holes should add these wind losses to the present estimate, not to speak of the radiative losses of the transition region. The flux we refer to is then the flux above the transition region. A rough estimate of the solar wind mass loss, deduced from an isothermal Parker model, say, is $4 \times 10^{-14} M_\odot$ yr^{-1} and the specific energy carried away by the wind is almost entirely kinetic at the orbit of earth with an observed velocity of about 400 km s^{-1}. This corresponds to an average energy flux at the solar surface of 7×10^4 ergs cm^{-2} s^{-1}. Added to our estimated conductive losses, we find the sum to be just a little less than 10^5 ergs cm^{-2} s^{-1}, even when the location of the temperature maximum is higher, and definitely larger than 10^5 ergs cm^{-2} s^{-1} when it is lower.

The most robust conclusion of this discussion of the open corona is that the height up to which the plasma is heated is larger than the height at which the temperature reaches a maximum. We have proved this to be true (from eq. [5.10]) whatever the distribution of the heating rate versus height. A temperature maximum at about 1.5 $R_\odot$ corresponds to a heating region between the base and an altitude of about 0.5 to 0.7 $R_\odot$. Our particular choice of heating profile places the upper limit of the heating zone at an altitude of 0.7 $R_\odot$ for a maximum temperature at 0.5 $R_\odot$ above the solar surface.

6. GLOBAL BEHAVIOR OF THE SOLAR CORONA

Acton (1996) and Culhane (1997) have described the global features of the solar corona as determined from *Yohkoh*, which was launched on 1991 August 30. Since then the Soft X-Ray Telescope (SXT) has given a detailed record of the way the X-ray corona changes during the declining phase of the solar cycle. It images the Sun with an effective angular resolution of about 5″ out to about 1 $R_\odot$ above the limb and reveals that the emission is extremely inhomogeneous: over one-half of the X-ray flux comes typically from less than 2% of the image, namely, from active regions. Several images are taken every hour, giving a total of 10^5 over the 4 yr period.

Acton plots a variety of parameters as a function of time and finds that many of them follow the cycle. For example, the global X-ray intensity and global photospheric magnetic flux both decline by a factor of about 50–100. However, there is an unexpectedly low correlation with the

mean coronal temperature, which only changes a little from about 3 to about 2.5 MK. It is clear that the coronal emission is highly localized in nature and associated mainly with active regions.

Culhane (1997) focuses on the large-scale diffuse emission. He also stresses that near sunspot maximum the X-ray radiation is dominated by localized structures (active regions), whereas near sunspot minimum it is less concentrated and comes from large-scale diffuse structures. Most of the diffuse emission arises from closed magnetic arcades underlying helmet streamers, in which the temperature rises to a maximum of 2.2–2.3 MK at about 1.5 $R_\odot$. By comparison the temperature in coronal holes levels off at about 1.5 MK, also at about 1.5 $R_\odot$. Further puzzling properties are that the density (as measured by the square root of the emission measure) declines steadily by a factor of 1.01 and that it is not hydrostatic.

In order to have an understanding of the global solar corona that is sufficiently robust to be extrapolated to other stars (Jordan 1997) we need to answer at least the following simple questions.

1. Why does the coronal intensity decline by about a factor of 100 from sunspot maximum to sunspot minimum?
2. Why is the maximum temperature in closed regions 2.2–2.3 MK and why does it occur at about 1.5 $R_\odot$?
3. Why is the maximum temperature in coronal holes 1.5 MK and why does it occur at about 1.5 $R_\odot$?

6.1. *Global Coronal Emission*

The first question may be understood as follows. Let us write the global coronal intensity

$$I = I_q + I_{\rm ar} \tag{6.1}$$

as the sum of a background quiet diffuse term (I_q) and an active-region contribution ($I_{\rm ar}$). Now, whether the heating is produced by a mechanism that is essentially MHD waves, current sheets, magnetic reconnection or MHD turbulence, in each case the energy flux through the photosphere due to surface motions moving around magnetic field lines either rapidly or slowly is just the Poynting flux through the solar surface. Since the Poynting flux due to a velocity $\boldsymbol{v}$ acting on a magnetic field $\boldsymbol{B}$ is of order vB^2/μ per unit area, these may in turn be written as

$$I_q = 4\pi R_\odot^2 \frac{vB_q^2}{\mu}\,, \quad I_{\rm ar} = 4\pi f R_\odot^2 \frac{vB_{\rm ar}^2}{\mu}\,, \tag{6.2}$$

where B_q and $B_{\rm ar}$ are the photospheric fields in the quiet Sun and in active regions and f is the fraction of the solar surface covered by active regions. Thus, if we denote values at sunspot maximum by a subscript "max" and at sunspot minimum by a subscript "min" (when f vanishes), the ratio of the global coronal intensities at maximum and minimum may be written

$$\frac{I_{\rm max}}{I_{\rm min}} = \frac{B_{q\,\rm max}^2}{B_{q\,\rm min}^2} + \frac{f_{\rm max} B_{ar\,\rm max}^2}{B_{q\,\rm min}^2}\,. \tag{6.3}$$

Now the ratio $B_{q\rm max}/B_{q\rm min}$ is roughly 1.5 (Harvey 1984), while $f_{\rm max}$ is about 0.1 (Acton 1996), and the ratio $B_{ar\rm max}/B_{q\rm min}$ is typically 30 (if $B_{ar\rm max} \approx 300$ G and $B_{q\rm min} \approx 10$ G), so

$$\frac{I_{\rm max}}{I_{\rm min}} \approx 90\,, \tag{6.4}$$

as required, and the contribution at sunspot maximum is dominated by active regions.

6.2. *Maximum Temperatures*

Why is the maximum temperature in large closed regions about 2.3 MK, whereas the maximum in coronal holes is about 1.5 MK?

The maximum temperature in diffuse loops must be higher than in holes, because in holes part of the dissipated energy flows away as solar wind losses, whereas in loops it goes away only as conducted flux. Let us quantify this difference as follows by using the observed temperatures to deduce the ratio ($F_w/F_{\rm op}$) of the wind losses to input Poynting flux. From the loop analysis above in § 2, the relation between the conductive flux at the base and the base temperature is from equation (2.4),

$$F_0 = H_0 L = \frac{2\kappa_0 T_0^{7/2} \overline{H}}{7L}\,, \tag{6.5}$$

where L is the loop length and T_0 the temperature at the base of the loop, while $\overline{H}$ is the dimensionless heating parameter defined in equation (2.6). Eliminating $\overline{H}$ from equation (6.5) and an expression for the loop summit temperature (T_m) for uniform heating from equation (2.7), we obtain the base-flux/summit-temperature relation as

$$F_0 = \frac{4\kappa_0}{7L}\,(T_m^{7/2} - T_0^{7/2})\,. \tag{6.6}$$

In open magnetic regions, the analysis of § 5 shows that the base conductive flux is given in terms of the parameter $F_0^* = (r^* - 1)$ by $F_0 = F_0^* H_0 L^2/R_\odot$. By using equation (5.11) this may be written in terms of the maximum temperature ($\overline{T}$) as

$$F_0 = \frac{2}{7}\,\kappa_0 \left(\frac{\overline{T}^{7/2} - T_0^{7/2}}{R_\odot}\right) \frac{F_0^*}{F_0^* - \log\,(1 + F_0^*)}\,. \tag{6.7}$$

However, F_0 is not the same in both cases because of wind losses. Whereas for the closed loop the base conducting flux is approximately the amount of Poynting flux ($F_{\rm cl}$) that enters the base of loops, for open regions the downward conducting flux equals the input Poynting flux ($F_{\rm op}$) minus the energy flux carried away by the solar wind (F_w). So we can write $F_{\rm cond} = F_{\rm op} - F_w$.

We can now calculate the ratio of conductive fluxes at the base of closed and open regions as

$$\frac{F_{\rm cond,\,cl}}{F_{\rm cond,\,op}} = \frac{2\,R_\odot}{L}\,\frac{\overline{T}_{\rm cl}^{7/2} - T_{0,\rm cl}^{7/2}}{\overline{T}_{\rm op}^{7/2} - T_{0,\rm op}^{7/2}}\,\frac{T_0^* - \ln(1 + T_0^*)}{T_0^*}\,. \tag{6.8}$$

Numerically, observations suggest the values $\overline{T}_{\rm cl} = 2.3$ MK, $T_{0,\rm cl} = 0.5$ MK, $\overline{T}_{\rm op} = 1.5$ MK, $T_{0,\rm op} = 0.5$ MK, while the value of the parameter T_0^* has been found to be about 0.5. If we take a loop length equal to 100,000 km, we obtain in numerical terms

$$\frac{F_{\rm cl}}{F_{\rm op} - F_w} = \frac{F_{\rm cond,\,cl}}{F_{\rm cond,\,op}} = 12\,. \tag{6.9}$$

The analysis of § 4.1 has also shown that the flux entering loops is of order 5×10^5 ergs cm^{-2} s^{-1}, while the total flux entering magnetically open regions is about 10^5 ergs cm^{-2} s^{-1}. Therefore, we also have $F_{\rm cl}/F_{\rm op} \approx 5$, which allows us to find F_w in terms of $F_{\rm op}$ from equation (6.9) as

$$F_w = 0.58 F_{\rm op}\,. \tag{6.10}$$

This is consistent with our above solar wind analysis. The rough estimate of solar wind losses was $F_w \approx 70{,}000$ ergs cm^{-2} s^{-1}, which should, according to the present discussion, be associated with a total Poynting flux of $F_{op} = 70{,}000/0.58 = 1.2 \times 10^5$ ergs cm^{-2} s^{-1}, leaving a conduction flux from the open corona to the Sun of $120{,}000 - 70{,}000 = 5 \times 10^4$ ergs cm^{-2} s^{-1}, whereas our analysis of the hole temperature data, with just these figures for base and maximum temperatures, has given a base conduction flux of 1.6×10^5 ergs cm^{-2} s^{-1}. The discrepancy is not considerable, given the uncertainties in hole measurements and the fact that the conductive flux also provides heating and radiation in the transition region. Since we already demanded $F_{cl}/F_{op} \approx 5$, the result is also consistent with our estimate of the conductive flux from loop temperature data.

7. CONCLUSION

We are suggesting a new approach to the coronal heating problem, namely, to split it into two parts and attempt to answer the following questions.

1. What form of heating $H(s)$ is producing the observed temperature profile in a loop or more generally in other coronal structures such as arcades?
2. What heating mechanism can produce the form of heating inferred in step 1?

Of course, if two forms of heating do not produce a significantly different temperature profile, then step 1 cannot distinguish between them. In addition, if two heating mechanisms produce the same heating form, then step 2 cannot itself determine which is most likely. Nevertheless, we are hopeful that this approach may narrow down the hunt for heating mechanisms very substantially and certainly rule out many previously viable possibilities.

Different forms of heating (step 1) have a distinctive effect on the profiles along a loop of both the heat flux and the temperature (T). When the heating is uniform along the loop and radiation is negligible, the heat flux is a linear function of distance, while $T^{7/2}$ increases quadratically. When the heating is uniform over a distance L_H from the loop base, $T^{7/2}$ remains constant beyond L_H. When the heating is instead uniform over a distance L_H either side of the loop summit, $T^{7/2}$ declines linearly below L_H.

The behavior of $T^{7/2}$ with height on the axis of an arcade provides further information about the nature of the heating. If the heat is distributed uniformly throughout the arcade $T^{7/2}$ increases quadratically with height, whereas if the heat is uniform within each loop and the base flux is the same from one loop to another then $T^{7/2}$ increases linearly with height. When the heating is deposited only near the base, the temperature becomes uniform at large heights, whereas when it is deposited only near the summits it becomes linear at large heights.

An independent question (step 2 above) is how the above heating form varies with several different heating mechanisms as follows.

1. For single-site magnetic reconnection, the heat is likely to be localized near the reconnection site such as the top of a loop, although the effect of slow shocks means that it may also be liberated some distance away.
2. For base heating in a loop by, for example, reconnection of low-lying fields or X-ray–bright points, the heat would be localized near the loop footpoints.
3. For nanoflaring produced by turbulent braiding and current sheet formation, the heat tends to be distributed rather uniformly.
4. For long-wavelength Alfvén waves, phase mixing or resonant absorption tends to produce a heating that is more intense near the summit for the fundamental mode since the wave amplitude is highest there.

We have compared our models with three separate sets of observations of the large-scale corona from *Yohkoh*. They give strong evidence against heating concentrated near the loop base and also suggest that heating uniformly distributed along the loop is more likely than heating concentrated at the summit. From the observed temperature as a function of height within an arcade, we deduce that the heating is much more likely to have the same flux on each loop than to be uniformly distributed throughout the arcade. Furthermore, an excellent fit is found with a heating that is proportional to the square of the magnetic field of a model arcade.

We therefore conclude that the heating is liberated in situ along the whole loop rather than being a steady response either to low-lying heating near the feet (case 2 above) or to reconnection or some other mechanism focused at the loop summit (case 1). What about the possibility of Alfvén wave heating? The Alfvén wave transit time along a loop of length 700 Mm with an Alfvén speed of 2000 km s^{-1}, say (corresponding to a magnetic field of 10 G and a density of 10^8 cm^{-3}), is

$$\tau_A = \frac{L}{v_A} = 350 \text{ s} .$$

Thus the fundamental frequency is in the region of granulation frequencies (300–600 s) where there is substantial photospheric power. A loop reacts to such boundary motions in an AC (wave) mode rather than a DC mode. Because the frequency of boundary motions matches the fundamental mode frequency, we deduce that the fundamental is likely to be excited in the loop, so this is at first sight a promising heating mechanism. However, phase mixing or resonant absorption is likely to produce a spatially nonuniform heating, with heat dumped preferentially near the summit (although this has yet to be confirmed by detailed numerical calculations).

Stochastic or turbulent reconnection in many small current sheets may, by contrast, be driven by much slower footpoint motions. For example, supergranular velocities of, say, 0.3 km s^{-1} over a distance of 30 Mm act on a timescale of 10^5 s (about 1 day). A similar timescale arises from the photospheric/coronal connectivity cutting of Title (private correspondence), whereby the coronal connections to the photosphere (the so-called magnetic carpet) are changed over a time of 1–2 days. These slow footpoint motions will tend to make the coronal field evolve through a series of equilibria that go turbulent, either because of braiding-induced current sheets or because of fine-scale MHD instabilities such as the tearing mode. Since the loop cross-sectional areas are relatively uniform, the braiding and turbulence is likely to be spread uniformly along a loop rather than being focused at the summit. Indeed, a recent three-dimensional resistive MHD numerical experiment of Galsgaard et al. (1999) produces a rather uniform ohmic heating. The mechanism that most closely fits the observations at present is therefore turbulent reconnection.

However, we cannot completely rule out wave heating since, on the one hand, future simulation may show it to be capable of producing uniform heating and, on the other hand, the observational errors of the data we have analyzed are not small enough to give strong evidence against a model with a weak (say, sinusoidal) concentration at the summit.

We have raised several key questions about the nature of the global corona. The reason for the decline in coronal intensity by 2 orders of magnitude from sunspot maximum to sunspot minimum seems to be because of the ratio of the Poynting Flux in active regions to the quiet Sun. The difference in maximum temperature in closed and open regions may be understood in terms of the difference in the roles of the conductive flux there. Why does the maximum temperature in coronal holes occur at about 1.5 $R_\odot$? The temporal frequency of photospheric oscillations peaks at about $\tau_A = 300$ s in association with granulation and this should drive Alfvén waves near such a frequency. The corresponding wavelength is $\lambda = v_A \tau_A \approx 150$ Mm for an Alfvén speed of 500 km s^{-1}. Alfvén waves dissipate by laminar phase mixing over a very large height of $(6\ \mathrm{Re})^{1/3}/2\pi$ wavelengths, where Re is the smaller of the viscous and magnetic Reynolds numbers. This gives a height of about 300λ for $\mathrm{Re} = 10^7$, say. However, instabilities enhance the dissipation very substantially (Heyvaerts & Priest 1983; Browning & Priest 1984) and enable the waves to dissipate in a few wavelengths. In particular, dissipation over a couple of wavelengths would produce a temperature maximum at about 1.5 $R_\odot$.

As we have seen, the variation with position of the heat flux and $T^{7/2}$ are sensitive diagnostics of the form of the coronal heating. A natural future strategy therefore to determine more about the coronal heating mechanisms has several elements. First of all, the spatial forms of the heating produced by different mechanisms and their dependence on field strength and other parameters such as temperature and density need to be determined more accurately from theoretical and computational analysis. Second, better models of the temperature structure within coronal loops and arcades produced by given heating forms need to be developed. For example, the three-dimensional temperature structure in potential and force-free models of observed regions could be produced and integrated along the line of sight to compare with the observations. The present relatively simple analysis is a preliminary but necessary step for that much more substantial analysis. Also, other effects in the energy balance could be included such as radiation and enthalpy flux as well as the effects of time dependence and flows. Third, techniques for determining the temperature structure as accurately as possible from *Yohkoh*, *TRACE*, and *SOHO* observations are a high priority. Finally, a theoretical determination of the other consequences of the different heating mechanisms needs to be undertaken together with their detailed observation from *SOHO*, including flows, jetting, and levels of turbulence.

We are most grateful to the UK Particle Physics and Astronomy Research Council for financial support and to S. T. Buckland, A. Hood, and R. Walsh for helpful discussions. Part of the work was carried out while one of us (J. L. C.) was a Visiting Professor at the Institute for Space and Astronautical Science (ISAS) of Japan. NASA supported the work of L. W. A. under contract NAS8-37334. The *Yohkoh* mission and its continued operation are projects of ISAS in Japan.

APPENDIX A

OTHER LOOP MODELS

Here we extend the analysis of § 2 to the cases when the heating decays exponentially away from the feet or summit. Suppose first that the heating in the left-hand leg of the loop is of the form

$$H = H_0\, e^{-s/L_H} \tag{A1}$$

when $0 \le s \le L$, so that it decays exponentially with distance over a length L_H from the footpoint. Then the heat flux becomes

$$F = -H_0\, L_H (e^{-s/L_H} - e^{-L/L_H})\,, \tag{A2}$$

whose absolute value decreases from a base value of $F_0 = H_0\, L_H(1 - e^{-L/L_H})$ over a scale L_H to zero at the loop summit (Fig. 2*a*, *dashed curve*). The corresponding temperature (Fig. 3*a*, *dashed curve*) is

$$T(s) = T_0\left[1 + \overline{H}\,\frac{L_H^2}{L^2}\left(1 - \frac{s}{L_H}\,e^{-L/L_H} - e^{-s/L_H}\right)\right]^{2/7}. \tag{A3}$$

Thus, the main characteristics of this and the previous form of heating is a flattening of the temperature profile near the summit.

Suppose next that the heating decays exponentially away from a summit value of H_0, say, over a distance L_H. Then the base heating is $H_0\, e^{-L/L_H}$ and the heat flux Figure 2*b* (*dashed curve*) is

$$F = -H_0\, L_H (1 - e^{(s-L)/L_H})\,, \tag{A4}$$

so its absolute value decreases from $F_0 = H_0\, L_H(1 - e^{-L/L_H})$ at the base to zero at the summit. The resulting temperature profile (Fig. 3*b*, *dashed curve*) is

$$T = T_0\left\{1 + \overline{H}\,\frac{L_H^2}{L^2}\left[\frac{s}{L_H} - e^{-L/L_H}(e^{s/L_H} - 1)\right]\right\}^{2/7}, \tag{A5}$$

with a maximum value at the summit that is always smaller than the uniform heating value. The characteristic of this type of heating is therefore a flattening of the heat flux at low heights and of the temperature profile at large heights.

APPENDIX B

OTHER SEMICIRCULAR ARCADE MODELS

Here we extend the analysis of § 4.1 to the cases when the heating decays exponentially away from the feet or summit. Suppose first that the heating in each loop decays exponentially from the feet (eq. [A1]) to give the loop temperature shown in (A4). The resulting arcade profile is

$$T_s = T_0\left\{1 + 2c_H \frac{h_H^2}{R_\odot^2}\left[1 - \left(1 + \frac{h}{h_H}\right)e^{-h/h_H}\right]\right\}^{2/7} \tag{B1}$$

or

$$T_s = T_0\left[1 + \frac{2c_F h_H}{R_\odot}\frac{1 - (1 + h/h_H)e^{-h/h_H}}{1 - e^{-h/h_H}}\right]^{2/7} \tag{B2}$$

for uniform-heat or uniform-flux arcades, respectively. Figures 4*a* and 4*b* show how the temperature profiles (*dashed curves*) for this and the uniform-flux arcade are similar to the previous case but with the jumps in temperature gradient smoothed off.

Second, suppose the heating in each loop decays exponentially away from the summit over a distance L_H, so that the loop profiles are given by (A5). The arcade profile is then

$$T_s = T_0\left\{1 + \frac{2c_H h_H^2}{R_\odot^2}\left[\left(\frac{h}{h_H} - 1\right) + e^{-h/h_H}\right]\right\}^{2/7} \tag{B3}$$

for a uniform-heat arcade (Fig. 4*c*, *dashed curve*) or

$$T_s = T_0\left[1 + \frac{2c_F h_H}{R_\odot}\frac{(h/h_H - 1) + e^{-h/h_H}}{1 - e^{-h/h_H}}\right]^{2/7} \tag{B4}$$

for a uniform-flux arcade (Fig. 4*d*, *dashed curve*). Again it can be seen how the exponential profile produces the same qualitative behavior as the piecewise constant profile but with the sudden changes smoothed away.

APPENDIX C

DIPOLE ARCADES

Following on from § 3.2, we consider here the potential magnetic field due to a dipole of moment m submerged a distance d, say, below the coronal base (Fig. 6*b*). Positions are measured in a polar coordinate system with the dipole moment at the origin and the angle θ measured from the horizontal direction, so that the polar field components are given by

$$B_r = \frac{\mu_0}{4\pi}\frac{2m}{r^3}\cos\theta\,, \qquad B_\theta = \frac{\mu_0}{4\pi}\frac{m}{r^3}\sin\theta\,. \tag{C1}$$

The distance $L(h)$ along a field line (whose summit height is h) from footpoint to summit is

$$L(h) = \tfrac{1}{2}(d + h)[C_0\sqrt{1 + 3C_0^2} + \log(\sqrt{3}C_0 + \sqrt{1 + 3C_0^2})]\,, \tag{C2}$$

where $C_0 = \{1 - [d/(d + h)]^{2/3}\}^{1/2}$. The way in which L increases with h is shown in Figure 6*b*: at low heights it again increases like $h^{1/2}$ and at large heights like h.

In calculating the temperature along such a loop we must take account of the variation in flux tube cross section $[A(s)]$. Because of flux conservation along a tube, $A(s)B(s)$ is constant, and equation (2.1) becomes (in terms of the position angle defined in Fig. 6*a*)

$$\frac{1}{\sin\theta}\frac{d}{d\theta}\left(\frac{\sin^6\theta}{1 + 3\cos^2\theta}\frac{1}{\sin\theta}\frac{dT^{7/2}}{d\theta}\right) = -\frac{7(d + h)^2 H(\theta)}{2\kappa_0}\sin^6\theta\,. \tag{C3}$$

In solving it, several different distributions of heating rate may be considered. If $H(\theta)$ is a constant (H_0) along a given field line (which we refer to as case α), this equation can be integrated to give the summit temperature (T_m) as a function of the temperature at the base, situated at an angle θ_0, as

$$T_m = T_0\left[1 + \frac{H_0(d + h)^2\cos^2\theta_0}{10\kappa_0 T_0^{7/2}\sin^4\theta_0}(64 + 32\sin^2\theta_0 - 11\sin^4\theta_0 - 15\sin^6\theta_0)\right]^{2/7}. \tag{C4}$$

If, on the other hand (case β), $H(\theta)$ is taken to be proportional to the square of the local magnetic field, as it would be if it were to scale as the local magnetic energy density, we find

$$T_m = T_0\left[1 + \frac{7H_{\rm top}(d+h)^2}{4\kappa_0 T_0^{7/2}} \frac{\cos^2\theta_0}{\sin^8\theta_0}\right]^{2/7} . \tag{C5}$$

This can be transformed into a temperature versus height relation by using the above expression for C_0.

The corresponding variation with height of the temperature in the midplane of an arcade of dipolar loops depends on how the volumetric heating rate varies not only along the length of the loops but also from one loop to another. We calculate below the variation with height of the temperature $T_s(h)$ at the summit of field lines culminating at height h in the three cases of

1. a uniform volumetric heating rate (H_0) in the arcade;
2. a uniform distribution of the heat flux (F_0) at the base; and
3. a distribution of the heat flux at the base proportional to the square of the base magnetic field (this being expected to be close to the real situation if the energy flux is in the form of a Poynting flux).

Each of cases 2 or 3 splits further into two subcases according to whether the heating rate is constant along each field line (case α) or proportional to the square of the local magnetic field (case β). Situation 1 corresponds to a uniform heating rate and simply gives rise to the following "arcade profile":

$$T_s^{7/2}(h) = T_0^{7/2} + T_0^{7/2} c_{H_0} \frac{4(d+h)^2}{70\pi^2 R_\odot^2} \frac{(d+h)^{4/3} - d^{2/3}(d+h)^{2/3}}{d^{4/3}} \left[64 + 32\left(\frac{d}{d+h}\right)^{2/3} - 11\left(\frac{d}{d+h}\right)^{4/3} - 15\left(\frac{d}{d+h}\right)^2\right] , \tag{C6}$$

where $c_{H_0} = (7\pi^2 H_0 R_\odot^2)/(16\kappa_0 T_0^{7/2})$.

When field lines are heated uniformly along their length and the heat flux at the base is also uniform (which corresponds to case $\alpha 2$), the arcade temperature at height h, which we define as the summit temperature of the loop that culminates at this height, is given by

$$T_s^{7/2}(h) = T_0^{7/2} + c_F T_0^{7/2} \frac{2(d+h)}{70\pi R_\odot} \frac{[d/(d+h)]^{2/3}\sqrt{1-[d/(d+h)]^{2/3}}}{\sqrt{4-3[d/(d+h)]^{2/3}}} \times \frac{64 + 32[d/(d+h)]^{2/3} - 11[d/(d+h)]^{4/3} - 15[d/(d+h)]^2}{[d/(d+h)]^{2/3} + (3/5)\{1-[d/(d+h)]^{2/3}\}^2 - (1/7)\{1-[d/(d+h)]^{2/3}\}^3} . \tag{C7}$$

When field lines are heated uniformly along their length and the heat flux at the base is proportional to the square of the base magnetic field (which corresponds to case $\alpha 3$), we obtain the arcade temperature at height h as

$$T_s^{7/2}(h) = T_0^{7/2} + c_{F_0} T_0^{7/2} \frac{2(d+h)}{70\pi R_\odot} \left(\frac{d}{d+h}\right)^{8/3} \sqrt{1-\left(\frac{d}{d+h}\right)^{2/3}} \sqrt{4-3\left(\frac{d}{d+h}\right)^{2/3}} \times \frac{64 + 32[d/(d+h)]^{2/3} - 11[d/(d+h)]^{4/3} - 15[d/(d+h)]^2}{[d/(d+h)]^{2/3} + (3/5)\{1-[d/(d+h)]^{2/3}\}^2 - (1/7)\{1-[d/(d+h)]^{2/3}\}^3} , \tag{C8}$$

where $c_{F_0} = (7F_0\pi R_\odot)/(8\kappa_0 T_0^{7/2})$.

When the volumetric heating rate is, along a given loop, proportional to the square of the local magnetic field, the flux at the base and the summit temperature (T_m) are given by equation (C4). With a uniform base flux F_0 (which corresponds to case $\beta 2$), the arcade temperature at height h is given by

$$T_s^{7/2} = T_0^{7/2}\left\{1 + c_{F_0} \frac{2(d+h)}{\pi R_\odot} \left(\frac{d}{d+h}\right)^{2/3} \frac{\sqrt{1-[d/(d+h)]^{2/3}}}{\sqrt{4-3[d/(d+h)]^{2/3}}}\right\} . \tag{C9}$$

If, on the other hand, it is assumed that the base flux is proportional to the square of the base field while still assuming the heating rate in each loop scales as the square of the local field (which corresponds to case $\beta 3$), the arcade temperature at height h is

$$T_s^{7/2} = T_0^{7/2}\left[1 + c_{F_0} \frac{2(d+h)}{\pi R_\odot} \sqrt{1-\left(\frac{d}{d+h}\right)^{2/3}} \sqrt{4-3\left(\frac{d}{d+h}\right)^{2/3}} \left(\frac{d}{d+h}\right)^{8/3}\right] . \tag{C10}$$

where $c_{F_0} = (7F_0\pi R_\odot)/(8\kappa_0 T_0^{7/2})$.

This completes our calculations of the arcade temperature profile with height in cases 2 and 3 for loop heating situations α and β described above.

REFERENCES

Acton, L. W. 1996, in ASP Conf. Ser. 109, Cool Stars, Stellar Systems, and the Sun, ed. R. Pallavacini & A. K. Dupree (San Francisco: ASP), 45
Browning, P. K., & Priest, E. R. 1984, A&A, 131, 283
Cally, P. 1991, J. Plasma Phys., 45, 453
Cargill, P. J. 1994a, Solar System Plasmas in Space and Time, ed. J. Burch & J. H. Waite (Washington, DC: Am. Geophys. Union), 21
Cargill, P. J. 1994b, ApJ, 422, 381
Chiuderi, C., Einaudi, G., & Toricelli-Ciamponi, G. 1981, A&A, 97, 27
Culhane, J. L. 1997, Adv. Space Res., 19, 1839
Einaudi, G., Velli, M., Politano, H., & Pouquet, A. 1996, ApJ, 457, L113
Foley, C. A. 1998, Ph.D. thesis, University College, London
Foley, C. A., Culhane, J. L., & Acton, L. W. 1997, ApJ, 491, 933

Foley, C. A., Culhane, J. L., Weston, D., Acton, L. W., & Hara, H. 2000, Sol. Phys., submitted
Galsgaard, K., Mackay, D., Priest, E. R., & Nordlund, A. 1999, Sol. Phys., 189, 95
Galsgaard, K., & Nordlund, A. 1996, J. Geophys. Res., 101, 13445
Goedbloed, J. P. 1983, Lecture Notes on Ideal MHD, Rijnhuizen Rep. 83
Goossens, M. 1991, in Advances in Solar System MHD, ed E. R. Priest & A. W. Hood (Cambridge: Cambridge Univ. Press), 137
Hara, H., Tsuneta, S., Saku, Acton, L. W., Bruner, M., Lemen, J. R., & Ogawara, Y. 1994, PASJ, 46, 493
Harvey, K. L. 1984, Proc. 4th European Meeting on Solar Physics (ESA SP-220; Noordwijk: ESA), 235
Hendrix, D. L., & Van Hoven, G. 1996, ApJ, 467, 887
Heyvaerts, J. 1990, in IAU Symp. 142, Basic Plasma Processes on the Sun, ed. E. R. Priest & V. Krishna (Dordrecht: Kluwer), 207
Heyvaerts, J., & Priest, E. R. 1983, A&A, 117, 220
———. 1984, A&A, 137, 63
———. 1993, ApJ, 390, 297
Hollweg, J. V. 1983, in Solar Wind 5, ed. M. Neugebauer (NASA CP-2280), 1
Hood, A. W., Ireland, J., & Priest, E. R. 1997, A&A, 318, 957
Ichimoto, K., et al. 1995, ApJ, 445, 978
Jordan, C. 1992, Mem. Soc. Astron. Italiana, 63, 605
———. 1997, Astron. Geophys., 38, 10
Kano, R., & Tsuneta, S. 1996, PASJ, 48, 535
Klimchuk, J. A., & Gary, D. E. 1995, ApJ, 445, 925
Klimchuk, J. A., Lemen, J. R., Feldman, U., Tsuneta, S., & Uchida, Y. 1992, PASJ, 44, L181
Klimchuk, J. A., & Porter, L. J. 1995, Nature, 377, 131
Ko, Y.-K., Fisk, L. A., Geiss, J., Gloeckler, G., Guhathakurta, M. 1997, Sol. Phys., 171, 345
Krucker, S., & Benz, A. O. 1998, ApJ, 501, L213
Low, B. C., & Wolfson, R. 1988, ApJ, 324, 574
Mason, H. E. 1995, Adv. Space Res., 15, 53
Neupert, W. M., et al. 1998, Sol. Phys., 183, 305
Ofman, L., Davila, J. M., & Steinolfson, R. S. 1995, ApJ, 444, 471
Ogawara, Y., Takano, T., Kato, T., Kosugi, T., Tsuneta, S., Watanabe, T., Kando, I., & Uchida, Y. 1991, Sol. Phys., 136, 1
Parker, E. N. 1979, Cosmical Magnetic Fields (Oxford: Oxford Univ. Press)
———. 1990, Geophys. Astrophys. Fluid Dyn., 52, 183
———. 1994, Spontaneous Current Sheets in Magnetic Fields (Oxford: Oxford Univ. Press)
Parnell, C. E., Golub, L., & Priest, E. R. 1994, Sol. Phys., 151, 57
Parnell, C. E., & Jupp, P. E. 2000, ApJ, 529, 554
Poedts, S., Kerner, W., & Goossens, M. 1989, J. Plasma Phys., 42, 27
Porter, L. J., & Klimchuk, J. A. 1995, ApJ, 454, 499
Porter, L. J., Klimchuk, J. A., & Sturrock, P. A. 1994, ApJ, 435, 482
Priest, E. R. 1993, in Physics of Solar and Stellar Coronae, ed J. Linsky & S. Serio (Dordrecht: Kluwer), 515
———. 1996, Ap&SS, 237, 49
Priest, E. R., & Forbes, T. G. 2000, Magnetic Reconnection: MHD Theory and Applications (Cambridge: Cambridge Univ. Press)
Priest, E. R., Parnell, C. E., & Martin, S. F. 1994, ApJ, 427, 459
Roberts, B. 1984, in Hydromagnetics of Sun (ESA SP-220; Noordwijk: ESA), 137
Rosner, R., Tucker, W. H., & Vaiana, G. S. 1978, ApJ, 220, 643
Sakurai, T. 1985, in Theoretical Problems in High-Resolution Solar Physics, ed. H. Schmidt (MPA-212; Munich: MPA), 263
Shibata, K., Masuda, S., Shimojo, M., Hara, H., Yokoyama, T., Tsuneta, S., Kosugi, T., & Ogawara, Y. 1995, ApJ, 451, L83
Shimizu, T., Tsuneta, S., Acton L. W., Lemen, J. R., & Uchida, Y. 1992, PASJ, 4, L147
Steinolfson, R. S., & Davila, J. M. 1993, ApJ, 415, 354
Sturrock, P. A., Wheatland, M. S., & Acton, L. W. 1996, ApJ, 461, L115
Tataronis, J., & Grossman, W. 1973, Z. Phys., 261, 203
Tsuneta, S. 1996, in Solar and Astrophysical MHD Flows, ed K. Tsinganos (Dordrecht: Kluwer), 85
Tsuneta, S., & Lemen, J. R. 1993, in Physics of Solar and Stellar Coronae, ed J. Linsky & S. Serio (Dordrecht: Kluwer), 113
Tsuneta, S., Takatiashi, T., Acton, L. W., Bruner, M. E., Harvey, K., & Ogawara, Y. 1992, PASJ, 44, L211
Tsuneta, S., et al. 1991, Sol. Phys., 136, 37
Uchida, Y. 1993, in Physics of Solar and Stellar Coronae, ed J. K. Linsky & S. Serio (Dordrecht: Kluwer), 97
Ulmschneider, P., Priest, E. R., & Rosner, R. 1991, Mechanisms of Chromospheric and Coronal Heating (Berlin: Springer)
Vekstein, G., & Priest, E. R. 1992, ApJ, 384, 333
Vlahos, L. 1994, Space Sci. Rev., 68, 39
Waljeski, K., Dere, K. P., & Moses, D. 1992, Proc. 1st *SOHO* Workshop (ESA SP-348; Noordwijk: ESA), 281
Withbroe, G. L. 1988, ApJ, 267, 442
Yoshida, T., & Tsuneta, S. 1996, ApJ, 459, 342
Yoshida, T., Tsuneta, S., Golub, L., Strong, K. T., & Ogawara, Y. 1995, PASJ, 47, L15
Zirker, J. B. 1993, Sol. Phys., 148, 43